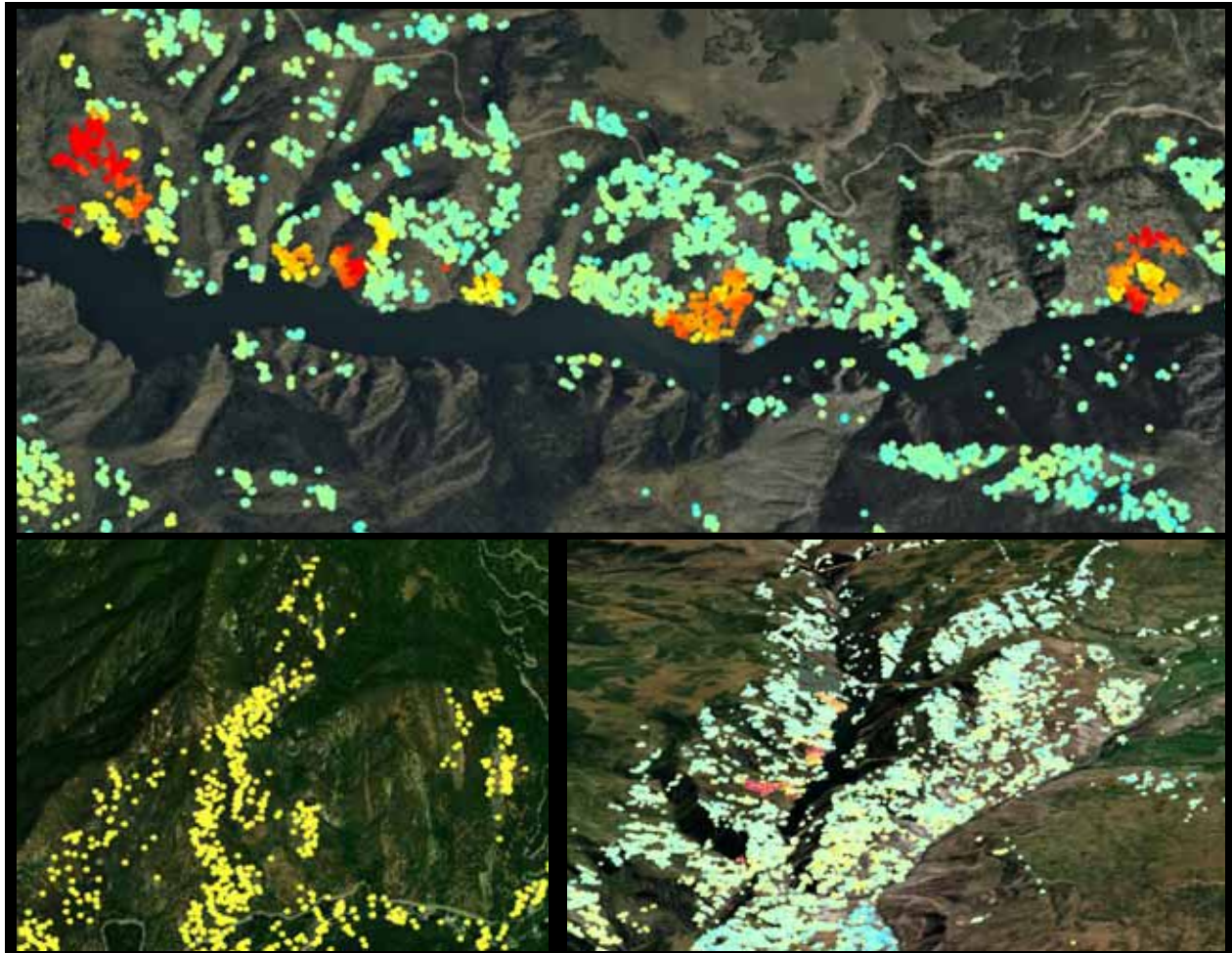

ADVANCED INSAR TECHNOLOGY (SQUEESAR™) For Monitoring Movement of Landslides

Publication No. FHWA-CFL/TD-11-005

September 2011



U.S. Department
of Transportation
**Federal Highway
Administration**

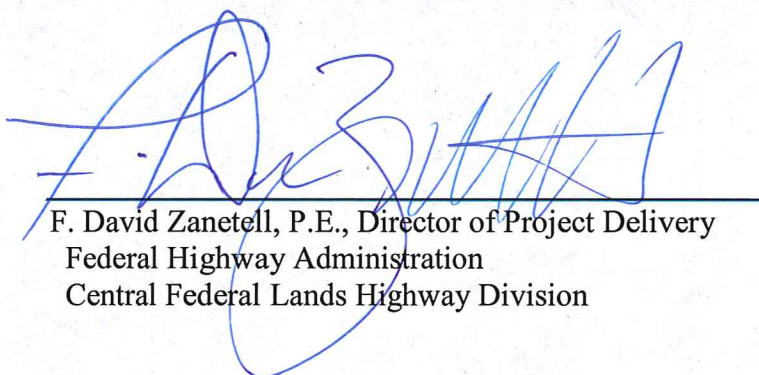


**Central Federal Lands Highway Division
12300 West Dakota Avenue
Lakewood, CO 80228**

FOREWORD

Synthetic aperture radar interferometry, also referred to as InSAR, is a method for measuring ground movement (changes in surface topography) over time. While traditional InSAR approaches such as DInSAR provide remote estimates of ground movement over large areas, these techniques have been limited in accuracy (centimeter scale precision) and results are often difficult to interpret. The recent development of advanced algorithms has significantly improved upon traditional InSAR methods by increasing the accuracy of results (millimeter scale precision) and providing individual measurement points, often with a high spatial density, over both urban and rural areas.

Several projects have been sponsored by the Federal Highway Administration (FHWA) in the past to demonstrate the use of InSAR technology at sites where landslides have been a regular disruptive feature on highway infrastructure within federal lands. While the objective of these projects was to evaluate the effectiveness of InSAR for monitoring slide movements, these demonstrations were primarily limited to DInSAR. Given the continued interest by the FHWA in monitoring landslide movement, the objective of this project was to revisit two of these landslide sites to test the use of the SqueeSAR™ algorithm, an advanced InSAR algorithm, for monitoring displacement.



F. David Zanetell, P.E., Director of Project Delivery
Federal Highway Administration
Central Federal Lands Highway Division

Notice

This document is disseminated under the sponsorship of the U.S. Department of Transportation in the interest of information exchange. The U.S. Government assumes no liability for the use of the information contained in this document.

The U.S. Government does not endorse products or manufacturers. Trademark or manufacturers' name appear in the document only because they are considered essential to the objective of the document.

Quality Assurance Statement

The FHWA provides high-quality information to serve Government, industry, and the public in a manner that promotes public understanding. Standards and policies are used to ensure and maximize the quality, objectivity, utility, and integrity of its information. The FHWA periodically reviews quality issues and adjusts its program and processes to ensure continuous quality improvement.

Technical Report Documentation Page

1. Report No. FHWA-CFL/TD-11-005	2. Government Accession No.	3. Recipient's Catalog No.	
4. Title and Subtitle <i>Advanced InSAR Technology (SqueeSAR™) For Monitoring Movement of Landslides</i>		5. Report Date September 2011	
		6. Performing Organization Code	
7. Author(s) Jessica Morgan, Giacomo Falorni, Adrian Bohane, (TRE Canada Inc.), Fabrizio Novali (Tele-Rilevamento Europa - T.R.E. s.r.l.,)		8. Performing Organization Report No. JO10-3025	
9. Performing Organization Name and Address TRE Canada Inc. thru: Yeh and Associates, Inc 409 Granville Street, Suite 550 5700 E. Evans Avenue Vancouver, BC V6C 1T2 Denver, CO 80222		10. Work Unit No. (TRAIS)	
		11. Contract or Grant No. DTFH68-07-D-00001	
12. Sponsoring Agency Name and Address Federal Highway Administration Central Federal Lands Highway Division 12300 W. Dakota Avenue, Suite 210 Lakewood, CO 80228		13. Type of Report and Period Covered Final Report September 2010 – April 2011	
		14. Sponsoring Agency Code HFTS-16.4	
15. Supplementary Notes COTR: Roger Surdahl, FHWA-CFLHD. Advisory Panel Members: Alan Blair, FHWA-CFLHD; Scott Anderson and Barry Siel, FHWA-RC; David Lofgren, FHWA-WFLHD; Rick Andrew and Howard Hume, Yeh and Associates. This project was funded under the FHWA Federal Lands Highway Coordinated Technology Implementation Program (CTIP).			
16. Abstract Landslides are destructive natural hazards that can impact highway infrastructure within federal lands. InSAR technology can be used to monitor landslide movement, which has been demonstrated in previous projects sponsored by the FHWA. However, these demonstrations have been mainly limited to traditional InSAR methods. The SqueeSAR™ algorithm uses distinct properties of the signal from radar satellites, to detect millimeter-scale changes in the Earth's surface from natural and man-made features on the ground, representing a significant breakthrough in InSAR technology. This approach represents a significant advancement in the field of InSAR and has been successful in providing a more accurate overview of surface movement at other landslide sites under suitable conditions. Given the continued interest by the FHWA in the use of InSAR for natural hazard monitoring, the objective of this project was to test the use of the SqueeSAR™ algorithm for measuring landslide movement. Two sites previously analyzed using more traditional InSAR approaches were revisited with the SqueeSAR™ algorithm; the Amphitheatre Point Landslide (36.5426N, 118.7840W) in California and the Cimarron Landslide (38.3561N, 107.5823W) in Colorado. While the accuracy and density of measurement points identified in surrounding areas was quite high, the coverage of identified targets was limited within the two areas of interest. These limitations were the result of considerable environmental challenges at both sites. The Amphitheatre Point Landslide was located in a densely forested area of steep and variable topography, while the Cimarron Landslide site was also characterized by significant vegetation coverage. Despite the lack of results at the two landslides of interest, the effectiveness of the SqueeSAR™ approach was still demonstrated by identifying and measuring ground movement for a series of landslides near a reservoir north of the Cimarron Landslide site. The SqueeSAR™ technique is an algorithm for processing radar data that is based on a multi-interferogram approach and is the intellectual property of Tele-Rilevamento Europa - T.R.E. s.r.l.			
17. Key Words InSAR, SAR, SqueeSAR™, PSInSAR™, LANDSLIDES, GROUND MOVEMENT, SLOPE STABILITY, NATURAL HAZARD MONITORING		18. Distribution Statement No restriction. This document is available to the public from the sponsoring agency at the website http://www.cflhd.gov .	
19. Security Classif. (of this report) Unclassified	20. Security Classif. (of this page) Unclassified	21. No. of Pages 94	22. Price

SI* (MODERN METRIC) CONVERSION FACTORS

APPROXIMATE CONVERSIONS TO SI UNITS

Symbol	When You Know	Multiply By	To Find	Symbol
LENGTH				
in	inches	25.4	millimeters	mm
ft	feet	0.305	meters	m
yd	yards	0.914	meters	m
mi	miles	1.61	kilometers	km
AREA				
in ²	square inches	645.2	square millimeters	mm ²
ft ²	square feet	0.093	square meters	m ²
yd ²	square yard	0.836	square meters	m ²
ac	acres	0.405	hectares	ha
mi ²	square miles	2.59	square kilometers	km ²
VOLUME				
fl oz	fluid ounces	29.57	milliliters	mL
gal	gallons	3.785	liters	L
ft ³	cubic feet	0.028	cubic meters	m ³
yd ³	cubic yards	0.765	cubic meters	m ³
NOTE: volumes greater than 1000 L shall be shown in m ³				
MASS				
oz	ounces	28.35	grams	g
lb	pounds	0.454	kilograms	kg
T	short tons (2000 lb)	0.907	megagrams (or "metric ton")	Mg (or "t")
TEMPERATURE (exact degrees)				
°F	Fahrenheit	5 (F-32)/9 or (F-32)/1.8	Celsius	°C
ILLUMINATION				
fc	foot-candles	10.76	lux	lx
fl	foot-Lamberts	3.426	candela/m ²	cd/m ²
FORCE and PRESSURE or STRESS				
lbf	poundforce	4.45	newtons	N
lbf/in ²	poundforce per square inch	6.89	kilopascals	kPa
APPROXIMATE CONVERSIONS FROM SI UNITS				
Symbol	When You Know	Multiply By	To Find	Symbol
LENGTH				
mm	millimeters	0.039	inches	in
m	meters	3.28	feet	ft
m	meters	1.09	yards	yd
km	kilometers	0.621	miles	mi
AREA				
mm ²	square millimeters	0.0016	square inches	in ²
m ²	square meters	10.764	square feet	ft ²
m ²	square meters	1.195	square yards	yd ²
ha	hectares	2.47	acres	ac
km ²	square kilometers	0.386	square miles	mi ²
VOLUME				
mL	milliliters	0.034	fluid ounces	fl oz
L	liters	0.264	gallons	gal
m ³	cubic meters	35.314	cubic feet	ft ³
m ³	cubic meters	1.307	cubic yards	yd ³
MASS				
g	grams	0.035	ounces	oz
kg	kilograms	2.202	pounds	lb
Mg (or "t")	megagrams (or "metric ton")	1.103	short tons (2000 lb)	T
TEMPERATURE (exact degrees)				
°C	Celsius	1.8C+32	Fahrenheit	°F
ILLUMINATION				
lx	lux	0.0929	foot-candles	fc
cd/m ²	candela/m ²	0.2919	foot-Lamberts	fl
FORCE and PRESSURE or STRESS				
N	newtons	0.225	poundforce	lbf
kPa	kilopascals	0.145	poundforce per square inch	lbf/in ²

*SI is the symbol for the International System of Units. Appropriate rounding should be made to comply with Section 4 of ASTM E380.
(Revised March 2003)

TABLE OF CONTENTS

CHAPTER 1 – INTRODUCTION	1
STUDY OBJECTIVES AND SCOPE	1
BACKGROUND	2
InSAR	2
DInSAR	3
PSInSAR™.....	3
SqueeSAR™.....	3
PREVIOUS SATELLITE IMAGERY STUDIES PERFORMED	4
CHAPTER 2 – RADAR INTERFEROMETRY	7
METHODOLOGY	7
Master Image Selection	7
Signal Phase and Amplitude Analysis	8
Interferograms.....	9
Estimation of the atmospheric effects.....	9
Maximum Likelihood Analysis	10
Post-processing	10
AREAS OF INTEREST	11
Amphitheatre Point.....	11
Cimarron	13
RADAR DATA SELECTION	14
SENSITIVITY VERSORS	18
RADAR DATA ACQUISITION	19
CHAPTER 3 – RESULTS	21
REFERENCE POINT	21
DISPLACEMENT RATE	25
ELEVATION	27
ACCELERATION	29
OTHER PROPERTIES OF THE DATA	31
CHAPTER 4 – OBSERVATIONS	33
TARGET DISTRIBUTION AND DENSITY	33
Amphitheatre Point.....	33
Cimarron	37
LANDSLIDE MOVEMENT	40

Amphitheatre Point	40
MAXIMUM LIKELIHOOD RESULTS	41
ADDITIONAL OBSERVATIONS	45
Cimarron	45
CHAPTER 5 – PRECISION ASSESSMENT	49
GENERAL	49
PRECISION OF THE RESULTS	50
CHAPTER 6 – CONCLUSIONS	53
AMPHITHEATRE POINT	53
SqueeSAR.....	53
InSAR	53
CIMARRON	54
SqueeSAR.....	54
InSAR	54
CHAPTER 7 – RECOMMENDATIONS	57
BIBLIOGRAPHY	59
APPENDIX A – BASICS OF InSAR	63
INTERFEROMETRY	63
Interferograms.....	64
Contributors to Signal Phase	65
Coherence	66
DIFFERENTIAL InSAR (DInSAR)	67
INTERFEROGRAM STACKING	68
PERSISTENT SCATTERER TECHNIQUES	69
General Concept	69
Permanent Scatterers	69
Calculating Displacement.....	70
Precision	71
Validation of PS Data	72
Data Output and Presentation	73
SqueeSAR™	75
APPENDIX B – RADAR COHERENCE	77
APPENDIX C – AMPLITUDE MAPS	79

LIST OF FIGURES

Figure 1. Map. The location of the Amphitheatre Point Landslide (indicated with the red marker) in relation to the boundary of the Sequoia National Park (outlined in green). Kings Canyon National Park and the city of Visalia are also shown. 1

Figure 2. Map. The location of the Cimarron Landslide (indicated with the red marker). The Montrose county border and counties of the surrounding area are also shown. 2

Figure 3. Schematic. Illustration of the identification of permanent (PS) and distributed scatterers (DS) by the SqueeSAR™ algorithm. 4

Figure 4. Map. View of the AOI, as seen on Google Earth. 12

Figure 5. Map. View of the AOI, as seen on Google Earth. 13

Figure 6. Map. The coverage of the AOI by the satellite imagery. 14

Figure 7. Map. The coverage of the AOI by the satellite imagery. 15

Figure 8. Schematic. Geometry of the Envisat ascending image acquisitions over the Amphitheatre Point Landslide. θ is equal to 11.35° and represents the angle formed by the satellite with the north. δ is equal to 19.5° and represents the off-nadir angle formed by the beam. 16

Figure 9. Schematic. Geometry of the RADARSAT-1 descending image acquisitions over the Cimarron Landslide. θ is equal to 11.92° and represents the angle formed by the satellite with the north. δ is equal to 38.13° and represents the off-nadir angle formed by the beam. 17

Figure 10. Map. The location of the Amphitheatre Point Landslide reference point. 21

Figure 11. Map. Close-up of the Amphitheatre Point Landslide reference point. 22

Figure 12. Map. The location of the Cimarron Landslide reference point. 23

Figure 13. Map. Close up of the Cimarron Landslide reference point. 24

Figure 14. Map. PS and DS displacement rates for the Amphitheatre Point Landslide derived from the SqueeSAR™ analysis. 25

Figure 15. Map. PS and DS displacement rates for the Cimarron Landslide derived from the SqueeSAR™ analysis. 26

Figure 16. Map. PS and DS elevation for the Amphitheatre Point Landslide, displayed in meters above sea level. 27

Figure 17. Map. PS and DS elevation for the Cimarron Landslide, displayed in meters above sea level. 28

Figure 18. Map. PS and DS acceleration for the Amphitheatre Point Landslide, in mm/yr^2 29

Figure 19. Map. PS and DS acceleration for the Cimarron Landslide, in mm/yr^2 30

Figure 20. Map. Amplitude map (top panel) and an amplitude map with all identified PS and DS targets colored by displacement rates (bottom panel) shown for the area surrounding the Amphitheatre Point Landslide. 35

Figure 21. Map. Close-up of the amplitude map over the Amphitheatre Point Landslide AOI... 36

Figure 22. Map. Amplitude map (top panel) and an amplitude map with all identified PS and DS targets coloured by displacement rates (bottom panel) shown for the area surrounding the Cimarron Landslide. 38

Figure 23. Map. Close-up of the amplitude map over the Cimarron Landslide AOI. 39

Figure 24. Map. PS and DS displacement rates derived from the SqueeSAR™ analysis shown for the Amphitheatre Point Landslide AOI. 40

Figure 25. Map. Results of the SqueeSAR™ analysis (prior to data filtering for quality control) for the area surrounding the Amphitheatre Point Landslide AOI (top panel) and results of the Maximum Likelihood analysis for the same spatial extent. 43

Figure 26. Map. Results of the SqueeSAR™ analysis (prior to data filtering for quality control) for the area surrounding the Cimarron Landslide AOI (top panel) and results of the Maximum Likelihood analysis for the same spatial extent. 44

Figure 27. Map. PS and DS displacement rates derived from the SqueeSAR™ analysis shown for several landslides identified in the north portion of the radar scenes processed. 46

Figure 28. Graph. Time series for the point labeled TS1 in Figure 27. 47

Figure 29. Graph. Time series for the point labeled TS2 in Figure 27. 47

Figure 30. Graph. Time series for the point labeled TS3 in Figure 27. 47

Figure 31. Map. Standard deviation of the displacement rates estimated from the SqueeSAR™ data over the Amphitheatre Point Landslide area. 50

Figure 32. Map. Standard deviation of the displacement rates estimated from the SqueeSAR™ data over the Cimarron Landslide area. 51

Figure 33. Schematic. A schematic showing the relationship between ground displacement and signal phase shift. The numerical value of the wavelength is that of ERS. 63

Figure 34. Map. An interferogram generated from two radar images one of which was acquired before the L'Aquila earthquake (February 2009) and the other shortly after the event (April 2009). The fringes indicate coherence whereby displacement can be calculated in the corresponding areas. The areas with a spotty appearance are areas where decorrelation noise has occurred. Phase values range from $-\pi$ to $+\pi$ 65

Figure 35. Map. The visual display of results of a PSInSAR™ analysis of Lake Presenzano and its surrounding area. 70

Figure 36. Graph. A typical time series showing linear and non-linear patterns of movement. ... 71

Figure 37. Table. Typical values of precision (1 sigma) for a point less than 1 km from the reference point (P_0), considering a multi-year dataset of radar images. 72

Figure 38. Graph. Comparison of PSInSAR™ with GPS data. The x, y and z components of GPS measurements have been resolved to the equivalent LOS of the satellite data. 72

Figure 39. Graph. Optical leveling. The blue line is an optical benchmark correction curve; the red dots represent InSAR readings at the same location. 73

Figure 40. Graph. Thermal Dilation. Buildings move in response to changes in temperature and software is available to model such movement. The black line represents the results of a thermal dilation model while the red triangles correspond to InSAR readings on the same building, measured over the same time period..... 73

Figure 41 (a-c). Image. These images are screen-grabs from a GIS showing how distant and close-up views of deformation phenomena can be observed using GIS platforms. 74

Figure 42. Schematic. Schematic showing the distribution of PS and DS over a typical AOI. PS are identified as single objects returning a strong signal to the satellite. DS are homogeneous areas or scattered outcrops. Areas heavily covered by vegetation do not return the satellite signal. 75

Figure 43. Map. Comparison between the number of ground points identified using PSInSAR™ (previous algorithm identifying only PS) and SqueeSAR™ (latest algorithm identifying both PS and DS). There is a significant increase in the number of identified ground points..... 76

Figure 44. Map. Coherence of the radar targets before data filtering within the processed Amphitheatre Point Landslide area..... 77

Figure 45. Map. Coherence of the radar targets within the processed Cimarron Landslide area. 78

Figure 46. Map. Multi-image reflectivity map of the Amphitheatre Point Landslide area. North is pointing to the right side of the image. 79

Figure 47. Map. Multi-image reflectivity map of the Cimarron Landslide area. North is pointing to the left side of the image..... 80

LIST OF TABLES

Table 1. Components of the LOS vector for this Amphitheatre Point Landslide study. 18

Table 2. Components of the LOS vector for this Cimarron Landslide study. 18

Table 3. Dates of the ENVISAT ascending images. The image used as the Master is shown in bold, while images that were ordered but not delivered are shown in red..... 19

Table 4. Dates of the RADARSAT-1 descending images. The image used as the Master is shown in bold. 20

Table 5. Statistics of the processed Amphitheatre Point Landslide data. 31

Table 6. Statistics of the processed Cimarron Landslide data. 32

LIST OF ABBREVIATIONS

APS	Atmospheric Phase Screen
ASAR	Advanced Synthetic Aperture Radar
AOI	Area Of Interest
DEM	Digital Elevation Model
DInSAR	Differential Interferometric SAR
ERS	Earth Resources Satellite
ESA	European Space Agency
FAR	False Alarm Rate
GCP	Ground Control Point
GIS	Geographic Information System
GPS	Global Positioning System
InSAR	Interferometric SAR
LOS	Line Of Sight
ML	Maximum Likelihood
MLS	Minimum Least Squares
PS	Permanent Scatterer(s)
PSI	Phase Stability Index
PSInSAR™	Permanent Scatterers SAR Interferometry
SAR	Synthetic Aperture Radar
SNR	Signal to Noise Ratio
SqueeSAR™	Advanced InSAR algorithm
TS	(Permanent Scatterer Displacement) Time Series

CHAPTER 1 – INTRODUCTION

STUDY OBJECTIVES AND SCOPE

The Federal Highway Administration (FHWA), Central Federal Lands Highway Division (CFLHD) is interested in the use of InSAR to monitor the movement of landslides impacting infrastructure under its jurisdiction. Several projects involving the evaluation of InSAR techniques as a monitoring tool have been sponsored by the CFLHD in the past: *InSAR Deformation Monitoring, Badlands National Park*; *InSAR Applications for Highway Transportation Projects*; and *InSAR Deformation Monitoring, General's Highway, Sequoia National Park*. These three previous studies are also available at www.cflhd.gov.

However, recently developed algorithms possess significant advances upon the InSAR approaches used in previous demonstration projects. The objective of this project was to apply an advanced InSAR technique, specifically the SqueeSAR™ algorithm, to monitor ground movement of two landslides in close proximity to highways.

This report describes the findings of the SqueeSAR™ analysis of the Amphitheatre Point Landslide in Sequoia National Park, California as shown in Figure 1 and the Cimarron Landslide in Montrose County, Colorado in Figure 2.



Figure 1. Map. The location of the Amphitheatre Point Landslide (indicated with the red marker) in relation to the boundary of the Sequoia National Park (outlined in green). Kings Canyon National Park and the city of Visalia are also shown.



Figure 2. Map. The location of the Cimarron Landslide (indicated with the red marker). The Montrose county border and counties of the surrounding area are also shown.

BACKGROUND

InSAR

Interferometric Synthetic Aperture Radar, also referred to as SAR interferometry or InSAR, is the measurement of signal phase change (interference) between radar images. When a point on the ground moves, the distance between the sensor and the point changes, thereby producing a corresponding shift in signal phase. This shift is used to quantify the ground movement.

An interferogram is a 2D representation of the difference in phase values. Variations of phase in an interferogram are identified by fringes, colored bands that indicate areas where movement is occurring and the rate of movement being experienced. The precision with which the movement can be measured is usually in the centimeter range as the phase shift is also impacted by topographic distortions, atmospheric effects, and other sources of noise.

DInSAR

When InSAR is used to identify and quantify ground movement the process is referred to as Differential InSAR (DInSAR). In DInSAR topographic effects are removed by using a DEM of the area of interest to create a differential interferogram.

DInSAR is still impacted by atmospheric effects, as there is no method for removing this signal phase contribution. It is a useful tool for identifying footprints of progressing movement and creating deformation maps. The limitations of DInSAR are its relatively low precision (centimeter scale) and that it cannot distinguish between linear and non-linear motion.

PSInSAR™

PSInSAR™ is an advanced form of DInSAR. The fundamental difference is that it uses multiple interferograms created from a stack of at least 15 radar images.

PSInSAR™ was developed to overcome the errors produced by atmospheric artefacts on signal phase. The PSInSAR™ algorithm automatically searches the interferograms for pixels that display stable radar reflectivity characteristics throughout every image of the dataset. In PSInSAR™ these pixels are referred to as Permanent Scatterers (PS). The result is the identification of a sparse grid of point-like targets on which an atmospheric correction procedure can be performed. Once these errors are removed, a history of motion can be created for each target, allowing the detection of both linear and non-linear motion.

The result is a sparse grid of PS that are color-coded according to their deformation rate and direction of movement. The information available for each PS includes its deformation rate, acceleration, total deformation, elevation, coherence as well as a time series of movement. PSInSAR™ measures ground movement with millimetre accuracy.

SqueeSAR™

PS are objects, such as buildings, fences, lampposts, transmission towers, crash barriers, rock outcrops, etc, that are excellent reflectors of radar microwaves. However, many other signals are also present in the processed data. These do not produce the same high signal-to-noise ratios of PS but are nonetheless distinguishable from the background noise. Upon further investigation it was found that the signals are reflected from extensive homogeneous areas where the back-scattered energy is less strong, but statistically consistent. These areas have been called distributed scatterers (DS) and correspond to rangeland, pastures, bare earth, scree, debris fields, and arid environments as illustrated in Figure 3.

The SqueeSAR™ algorithm was developed to process the signals reflected from these areas. As SqueeSAR™ incorporates PSInSAR™ no information is lost and movement measurement accuracy is unchanged.

SqueeSAR™ also produces improvements in the quality of the displacement time series (records of movement over time at a specific radar target). The homogeneous areas that produce DS

normally comprise several pixels. The single time series attributed to each DS is estimated by averaging the time series of all pixels within the DS, effectively reducing noise in the data.

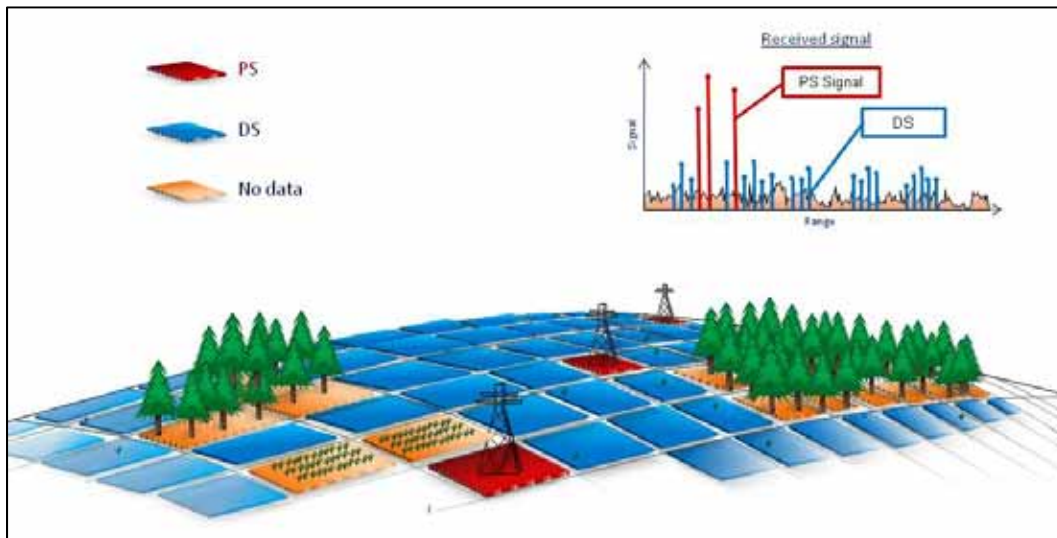


Figure 3. Schematic. Illustration of the identification of permanent (PS) and distributed scatterers (DS) by the SqueeSAR™ algorithm.

PREVIOUS SATELLITE IMAGERY STUDIES PERFORMED

InSAR Applications for Highway Transportation Projects (Cimarron Slide)

The project objective was to establish and demonstrate reliable, cost effective procedures to measure ground movement using InSAR in support of FLH projects. This report describes the effectiveness of InSAR in monitoring ground movement, and recommends guidelines for the coordinated use of InSAR with other FLH data collections, including photogrammetry, field surveys, boreholes and slope inclinometers. The study involved collection and analysis of InSAR data from both the past and present at three sites. The first site, the Prosser Slide in Benton County, Washington, provided a site with excellent InSAR coherence and gradual creeping movement that demonstrated the limits of InSAR movement measurement. The combination of a set of InSAR movement mapped over a two-year period, produced movement on the order of several centimeters that qualitatively correlated well with site observations and slope inclinometer measurements. The second slope, the Cimarron Slide in Owl Creek, Colorado, exhibited moderate coherence and highly visible InSAR movement signatures were produced over periods of several months. The third site, in Mesa Verde National Park near Cortez, Colorado, is a region of significant topographic relief, which made the use of satellite-based InSAR a challenge.

InSAR Deformation Monitoring, General's Highway, Sequoia National Park (Amphitheatre Slide)

The objective of this project was to provide measurements of the deformation that occurred at the Amphitheatre Slide using InSAR monitoring. Two strategies were followed: (i) Three Corner Reflectors (CR) were deployed, analyzed, and measured, which provided precise deformation measurements at their locations; (ii) conventional InSAR deformation maps were produced when possible, which depended on the level of temporal de-correlation in the data. The contract deliverables included deformation maps quantifying movement that occurred in 2007. For this study deformation maps and deformation profiles were produced for four measurement times focused on the three CRs. The study area corresponded to the area of the current investigation. At the time the CRs were installed, their latitude and longitude were recorded using a hand-held GPS unit but their vertical component of elevation was not reported at that time. Subsequently, their heights were obtained from the USGS 10 m DEM data, interpolated at the given coordinates. The CR positions used in this study are shown as the white triangle in Figure 4. The observed down-hill deformation had a maximum of 2.5 mm for CR#2 (Upper Slide Reflector) and 1.7 mm at CR#3 (Lower Slide Reflector), relative to the reference CR#1 (Stable Reflector), which was assumed to be not moving. The precision of the deformation measurements is computed as approximately 0.9 mm. The CRs were removed on August 6, 2008.

Further information on InSAR can be found in Appendix A.

CHAPTER 2 – RADAR INTERFEROMETRY

METHODOLOGY

The identification of PS and DS in a series of radar images comprises a sequence of steps. (Additional information is provided in Appendix A).

First, all radar data archives are screened to determine the most suitable source of raw data for the particular area of interest and to select all the high quality images within the chosen dataset.

As the signal echo from a single point target contains many returning radar pulses it appears defocused in a synthetic aperture radar (SAR) raw image. The first processing step is therefore to focus all the received energy from a target in one pixel. The images are then precisely aligned to each other, or co-registered, and analysed for their suitability for interferometry. The parameters that are analyzed are the normal baseline and the temporal distribution of the images.

There then follows a number of statistical analyses on the phase and amplitude characteristics of the backscattered radar signal that return to the satellite. If a concentrated number of signals reflect off a particular feature within a pixel and backscatter to the satellite, the feature is referred to as a ‘scatterer’. When the same scatterer appears in all, or most, of a data set of SAR images of a particular location, then the scatterer is deemed to be ‘permanent’.

At this stage it is possible to identify a subset of pixels, referred to as Permanent Scatterer Candidates (PSC), that are used to estimate the impact on signal phase of ionospheric, tropospheric and atmospheric effects, as well as possible orbit errors.

Once the signal phase has been corrected for these effects, any remaining changes in signal phase directly reflect ground movement.

Master Image Selection

SqueeSAR™ requires that one image (or scene) in each dataset has to become both a geometric and temporal reference to which all the other images are then related. This image is referred to as the master image and those that remain are slave images.

The master image should be chosen according to the following criteria:

- it minimises the spread of normal baseline values for the slave images;
- similarly, it minimises the temporal baseline values between the master and each slave image; and
- it minimises the effects of signal noise arising from changes in vegetation cover and/or small changes in the look angle of the satellite from one scene to another.

Signal Phase and Amplitude Analysis

General

Each pixel of a SAR image contains information on the amplitude of signals that are backscattered toward the satellite, as well as on the signal phase. The amplitude is a measure of the amount of the radar pulse energy reflected, while the phase is related to the length of the path of the electromagnetic wave, from the platform to the ground and back again.

Analyses of both amplitude and phase of the SAR image provide an indication of the stability of each pixel, over time, whereby it is possible to identify those pixels that are most likely to behave as Permanent Scatterers. Statistical methods are used extensively in this process.

Among the different statistical parameters that can be computed two are of particular interest: the Phase Stability Index (PSI), obtained from the phases of the images within the dataset, and the Multi Image Reflectivity (MIR) map, derived from the amplitude values of the available acquisitions.

Radar Phase and Coherence

The phase stability is strongly linked to the concept of coherence. Pixels that consistently display high phase stability are said to be coherent. Coherence is measured by an index that ranges from 0 to 1. When a pixel is completely coherent, it will have a coherence value of 1.

Correspondingly, if a pixel has a low phase stability, its coherence index will be 0. In general, interferometry is successful when the coherence index lies between 0.5 and 1.0. Coherence values for the two selected areas are shown in Appendix B.

Radar Amplitude and Multi-Image Reflectivity

The amplitude of a pixel within a SAR image is the aggregate of the backscattered energy toward the satellite from within the pixel's equivalent land area. This equivalent land area is referred to as the radar resolution, and in the case of the Envisat satellite, it measures about 20 by 4 meters. In the case of the RADARSAT-1 satellite, it measures about 20 by 5 meters. It is necessary to look into the amplitude values of all the images in the dataset, in order to understand exactly what was seen by the satellite at the time of each acquisition.

If a target has experienced significant change in its surface characteristics it will exhibit variation in its reflectivity (electromagnetic response) between two acquisitions. In such circumstances, the possibility of detecting movement by means of SAR interferometry is seriously compromised. The signal phase difference between the two images now contains not only the contribution due to displacement, but also that due to the change in the reflectivity of the target. This prevents, in the worst case, the obtaining of any useful information on ground movement.

Accordingly, it is necessary to look into the amplitude values of all the images in the dataset, in order to understand exactly what was seen by the satellite at the time of each acquisition.

Another artefact linked to amplitude is known as speckle. Speckle is random noise that appears as a grainy salt and pepper texture in an amplitude image. This is caused by random interference from the multiple scattering returns that occur within each resolution cell. Speckle has an adverse impact on the quality and usefulness of SAR images. However, the higher the number of images taken of the same area at different times or from slightly different ‘look’ angles, the easier it is to reduce speckle. This increases the quality and level of details of the amplitude image enabling it to be used as a background layer for observing the presence of PS results.

The Multi Image Reflectivity (MIR) map is the means by which speckle reduction is accomplished. Averaging a number of images tends to negate the random amplitude variability, leaving the uniform amplitude level unchanged. It should be emphasized that the information in the MIR map is the reflectivity of each pixel, i.e. the ability to backscatter the incident wave toward the satellite. Flat surfaces (roads, highway, rivers, and lakes) act like a mirror, meaning that if their orientation is not exactly perpendicular to the incident wave negligible energy is reflected back to the sensor; they appear dark in the image. On the other hand, because of their irregular physical shape, metal structures or buildings reflect a significant portion of the incident signal back to the radar, resulting in very bright pixels in the MIR map.

The MIR image derived from the Amphitheatre Point Landslide image archive and the Cimarron Landslide image archive is shown in Appendix C.

Interferograms

After the statistical analyses of the SAR images have been completed, a set of differential interferograms is generated. This entails subtracting the phase of each slave image from the phase of the master image. In doing so, the difference in signal path length between the two images is calculated. This difference is related to possible ground motion.

In any SAR image, there are embedded topographic distortions that arise during image acquisition. These are removed using a reference Digital Elevation Model (DEM), leaving ground movement and the signal phase distortions arising from atmospheric effects as the only embedded variables.

The differential interferograms represent the starting point for applying the SqueeSAR™ approach.

Estimation of the atmospheric effects

When a radar signal enters and exits a moisture-bearing layer in the atmosphere, its wavelength can be affected, introducing potential errors into the signal path length. The removal of atmospheric impacts is fundamental for increasing the precision of ground movement measurement.

A sub-set of pixels, usually corresponding to buildings, lampposts, antennas, small structures and exposed rocks, is chosen from among those that have high PSI values. These are referred to as

PS Candidates (PSC). PSC density is, of course, higher in towns and cities rather than in forests and vegetated areas. However, it is often possible to obtain good PSC density in rural areas.

For each image, the atmospheric impacts are estimated at each PSC location. The process is statistically based and benefits in accuracy by the greater the number of available images for the analysis. By comparing the atmospheric contribution on neighbouring pixels that would be experiencing the same atmospheric conditions, the atmospheric contribution can be reconstructed over the whole image.

The processed dataset allows identification of a PSC cluster dense enough to identify and extract the atmospheric contribution over the entire area of interest.

Maximum Likelihood Analysis

In an effort to extract as much information over the area as possible, an additional approach was applied to the AOI. This secondary analysis was also used to verify the results obtained over the Amphitheatre Point Landslide and Cimarron Landslide areas.

The Maximum Likelihood (ML) technique is a highly localized analysis, which examines displacement information on a point-by-point basis (every cell of data within the radar scene). In this approach, the single interferogram with the highest coherence, or quality, is used to represent ground movement for every cell of data. In addition, any contributions from atmospheric effects are ignored due to the highly localized application of this approach. The result is a single image representing displacement measured only from the most coherent data.

By removing the constraint that every point must remain coherent throughout the entire stack of radar scenes (critical in the SqueeSARTM algorithm), the ML technique accounts for radar signal decorrelation throughout time. As a result, a secondary benefit of the ML approach is that the results provide an overview of the optimal coherence that can be obtained for any given site. In this regard, the results can be used to assess site coherence under the best possible circumstances.

It is important to note that there are several limitations inherent to the ML approach. First, it is not known which two scenes comprise the interferogram used to assign displacement values to each cell. As a result, the time interval over which ground displacement occurs is unknown and may vary across the end result. Furthermore, as numerous interferograms are used, the time of year may also fluctuate among ML data cells. Finally, as the product of an ML analysis is static, no time series information can be extracted.

Post-processing

In this stage the processed data undergoes a thorough quality control following ISO 9001:2000 guidelines. The PS data is checked for anomalies, aligned on an optical image layer and the final report is prepared.

AREAS OF INTEREST

Two sites were selected for analysis with SqueeSAR™, including the Amphitheatre Point Landslide (36.5426N, 118.7840W) located within Sequoia National Park, California and the Cimarron Landslide (38.3561N, 107.5823W) located within Montrose county, Colorado. These two sites were selected because they are locations of known slope instability and have been analyzed in a previous study using traditional InSAR techniques.

Amphitheatre Point

This landslide is located on fairly rugged terrain, with steep slopes characterizing most of the area of interest (AOI) and surrounding area. This is problematic for the application of InSAR, as steep topography can cause portions of the site to appear distorted or be completely hidden from the satellites field of view. In locations of mountainous terrain, the identification of radar targets is often challenging.

Vegetation is present throughout the AOI, which is another challenging characteristic for the application of InSAR. The changes in reflectivity exhibited by vegetation over time causes radar data captured over these areas to decorrelate, meaning InSAR analysis is often unsuccessful in densely vegetated areas.

As the landslide is located within a National Park, there are very few man-made structures within the AOI, with the exception of Highway 198 (Generals Highway) clearly visible in Figure 4. This limited the number of potential radar targets that could be established from anthropogenic structures, such as buildings. However, there are several natural features, including bare patches of ground or rocky outcrops that provided the basis for measurement points.

An AOI with a spatial extent of 0.459 mi² (1.19 km²) in size was defined around the body of this landslide as indicated in Figure 4.



Figure 4. Map. View of the AOI, as seen on Google Earth.

Cimarron

As seen in Figure 5, vegetation is fairly abundant throughout the western half and along the southern border of the Cimarron AOI. Similar to the Amphitheatre Point site, vegetation is highly problematic for the application of InSAR, meaning stable radar targets are challenging to identify.

With the exception of Cimarron Road (which intersects the body of the landslide approximately 10km down the road as the road branches south off of Highway 50), there are very few man-made structures within the AOI. This characteristic prevented the identification of numerous Permanent Scatterers (individual features or objects) from anthropogenic sources at this site, such as buildings.

This site is also subject to intermittent snow cover. Snow interrupts the radar signal by absorbing it, meaning data cannot be retrieved from images impacted by snow cover. Snowfall measured at a nearby weather station in Cimarron, CO recorded monthly totals exceeding 5 inches for at least 4 months of each year between 2003 and 2008 (years with complete weather records), which may have been a factor impeding InSAR analysis.

An AOI with a spatial extent of 0.683 mi^2 (1.77 km^2) in size was defined around the body of the landslide.



Figure 5. Map. View of the AOI, as seen on Google Earth.

RADAR DATA SELECTION

The radar dataset used to analyze the Amphitheatre Point site is from the ENVISAT satellite and comprises a total of 40 scenes. The images were acquired from Track 120 of an ascending orbit (satellite travelling from south to north). The coverage of the AOI by the satellite imagery is shown in Figure 6.



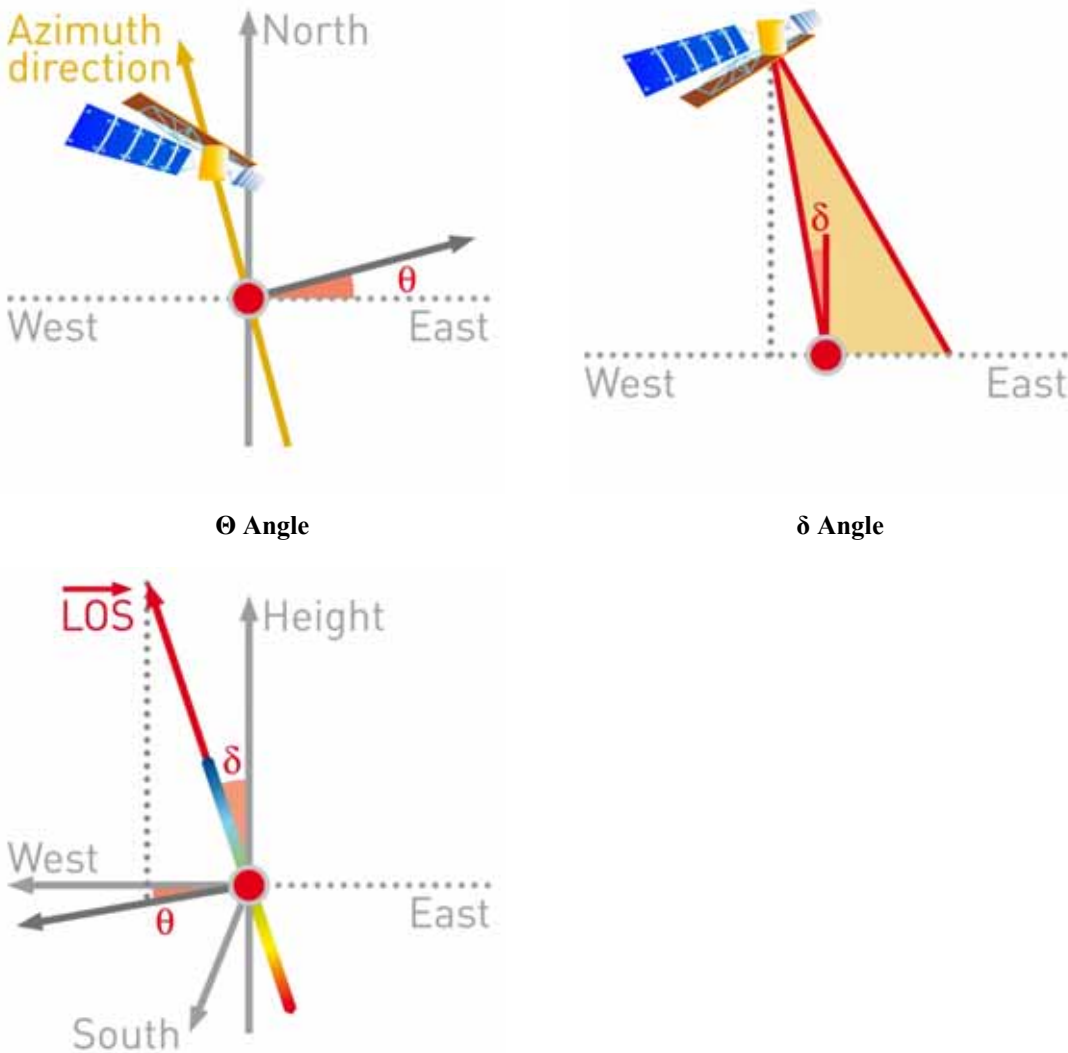
Figure 6. Map. The coverage of the AOI by the satellite imagery.

The radar dataset used for this analysis of the Cimarron Landslide is from the RADARSAT-1 satellite and comprises a total of 30 scenes. The images were acquired from Track 273 of a descending orbit (satellite travelling from north to south). The coverage of the AOI by the satellite imagery is shown in Figure 7.



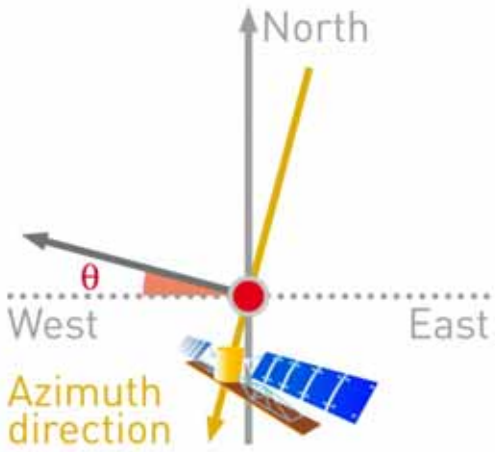
Figure 7. Map. The coverage of the AOI by the satellite imagery.

In all InSAR analyses the displacement measurements are one-dimensional and are carried out along the satellite line-of-sight (LOS). The LOS angle varies depending on the satellite and on the acquisition parameters. Another important parameter is the angle the satellite orbit forms with the geographic North. The geometry of the system used to capture images for the Amphitheatre Point radar dataset is shown in Figure 8. The geometry of the system used to capture images for the Cimarron radar dataset is shown in Figure 9. The symbol δ (delta) represents the LOS angle and Θ (theta) the angle with the North.

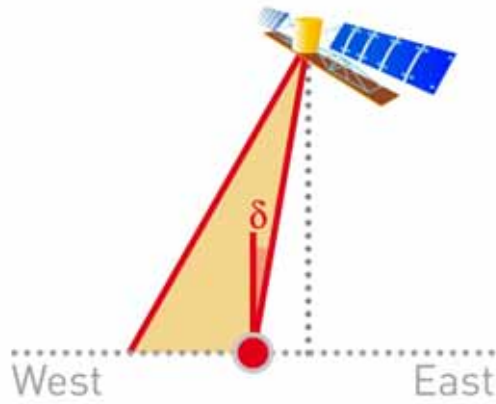


Line Of Sight

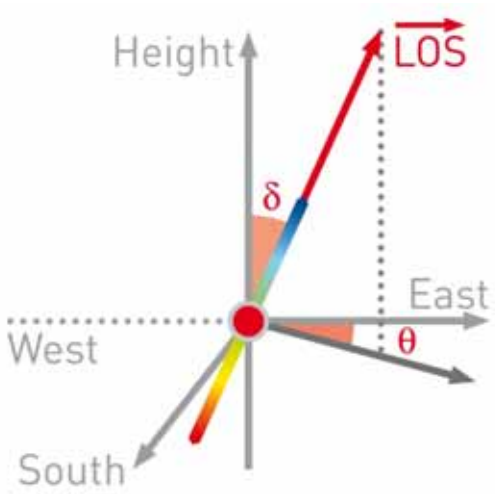
Figure 8. Schematic. Geometry of the Envisat ascending image acquisitions over the Amphitheatre Point Landslide. θ is equal to 11.35° and represents the angle formed by the satellite with the north. δ is equal to 19.5° and represents the off-nadir angle formed by the beam.



θ Angle



δ Angle



Line Of Sight

Figure 9. Schematic. Geometry of the RADARSAT-1 descending image acquisitions over the Cimarron Landslide. θ is equal to 11.92° and represents the angle formed by the satellite with the north. δ is equal to 38.13° and represents the off-nadir angle formed by the beam.

SENSITIVITY VERSORS

Table 1 contains the LOS versor properties for the Amphitheatre Point Landslide study, while Table 2 contains the LOS versor properties for the Cimarron Landslide. These values can be used to determine the sensitivity of the LOS to the vertical, East and North directions. As an example, consider the 19.5 off-nadir viewing angle. It is quite steep and gives rise to a versor value of 0.943 (obtained as the cosine of δ). This implies that the sensor is very sensitive to vertical motion. Conversely, the sensitivity to movement in the East-West direction is significantly lower (-0.327) and to the North-South direction lower yet (0.066).

Table 1. Components of the LOS versor for this Amphitheatre Point Landslide study.

Direction	Component of the versor
North	-0.06569
East	-0.32734
Vertical	0.94262

Table 2. Components of the LOS versor for this Cimarron Landslide study.

Direction	Component of the versor
North	-0.12755
East	-0.60417
Vertical	0.78658

RADAR DATA ACQUISITION

Of the 44 images originally ordered for the Amphitheatre Point area, four were not delivered by the vendor. All of the images that were delivered were suitable for InSAR processing. Table 3 lists the images used for this Amphitheatre Point project.

Data delivery issues are not uncommon with archive imagery. Unfortunately, it is not possible to know at the time the data is ordered which and how many of the images will not be delivered. The available images covered the period from 9 October 2003 to 24 February 2010. The Master image is shown in bold. This is used as the reference image for the analysis (see Appendix A for details).

Table 3. Dates of the ENVISAT ascending images. The image used as the Master is shown in bold, while images that were ordered but not delivered are shown in red.

ID	Date	ID	Date
1	29/10/2003	23	12/12/2007
2	30/06/2004	24	16/01/2008
3	08/09/2004	25	20/02/2008
4	13/10/2004	26	26/03/2008
5	17/11/2004	27	30/04/2008
6	22/12/2004	28	04/06/2008
7	02/03/2005	29	09/07/2008
8	11/05/2005	30	13/08/2008
9	15/06/2005	31	17/09/2008
10	20/07/2005	32	11/03/2009
11	07/12/2005	33	15/04/2009
12	11/01/2006	34	20/05/2009
13	15/02/2006	35	24/06/2009
14	22/03/2006	36	29/07/2009
15	26/04/2006	37	02/09/2009
16	31/05/2006	38	07/10/2009
17	18/10/2006	39	11/11/2009
18	27/12/2006	40	16/12/2009
19	25/07/2007	41	20/01/2010
20	29/08/2007	42	24/02/2010
21	03/10/2007	43	31/03/2010
22	07/11/2007	44	05/05/2010

Table 4 lists the images used for the Cimarron Landslide project. All of the images delivered by the vendor for this area were suitable for InSAR processing.

The available images covered the period from 29 December 2003 to 27 March 2010. The Master image is shown in bold. This is used as the reference image for the analysis (see Appendix A for details).

Table 4. Dates of the RADARSAT-1 descending images. The image used as the Master is shown in bold.

ID	Date	ID	Date
1	12/29/2003	21	4/25/2009
2	1/22/2004	22	6/12/2009
3	8/15/2006	23	7/30/2009
4	4/12/2007	24	9/16/2009
5	5/6/2007	25	11/3/2009
6	6/23/2007	26	11/27/2009
7	7/17/2007	27	1/14/2010
8	5/24/2008	28	2/7/2010
9	6/17/2008	29	3/3/2010
10	7/11/2008	30	3/27/2010
11	8/4/2008		
12	8/28/2008		
13	9/21/2008		
14	10/15/2008		
15	11/8/2008		
16	12/2/2008		
17	12/26/2008		
18	1/19/2009		
19	2/12/2009		
20	3/8/2009		

CHAPTER 3 – RESULTS

REFERENCE POINT

SqueeSAR™ is a differential technique: displacement is measured compared to a reference point that is assumed to be stable.

In the case of the Amphitheatre Point Landslide, the reference point could not be located within the AOI, because of the general instability of the site. As a result, the reference point was placed in a location which displayed very little movement over the time period monitored, and was therefore assumed to be motionless. Due to the limited number of radar targets identified near the AOI, the reference point was located approximately 10 km away.

The reference point location for the Amphitheatre Point Landslide is shown in Figure 10. A close up of the reference point is shown in Figure 11. Exact coordinates of the reference point are listed in Table 5.

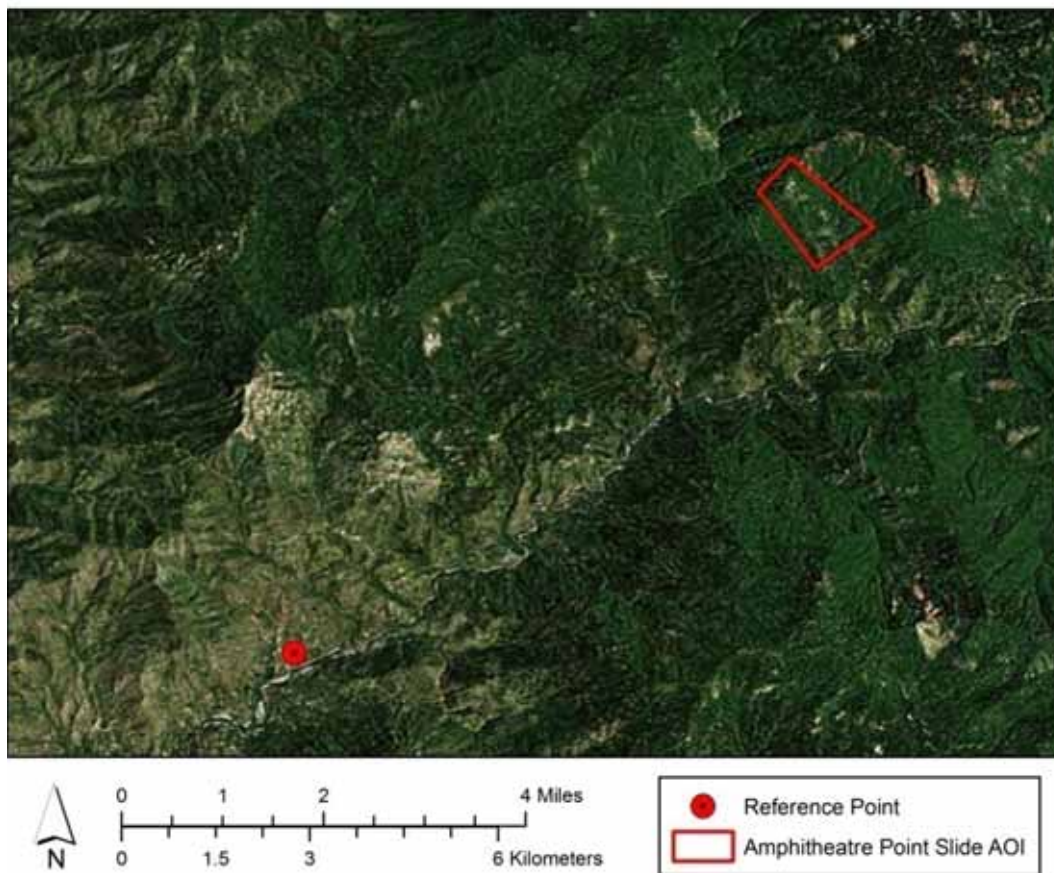


Figure 10. Map. The location of the Amphitheatre Point Landslide reference point.

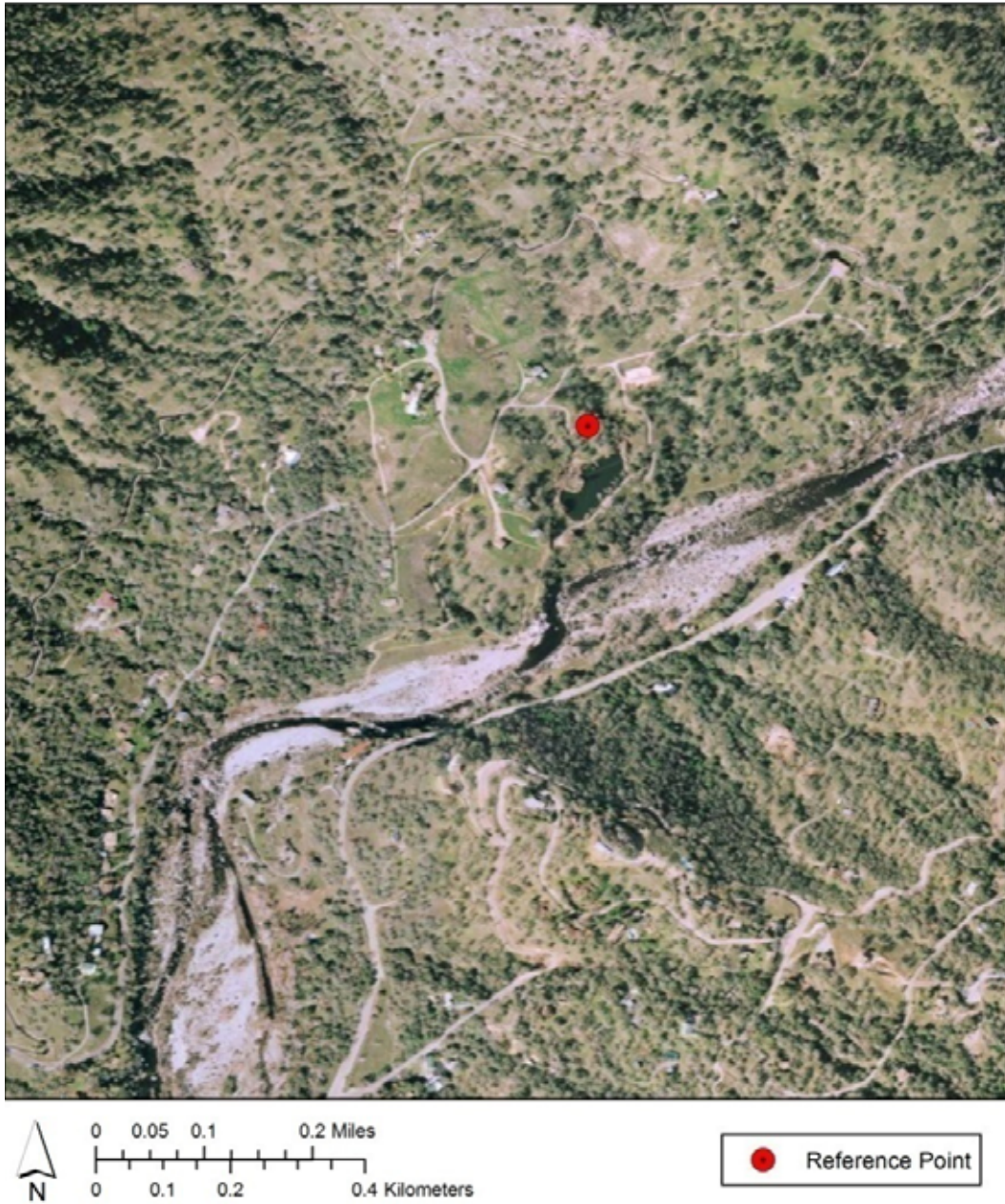


Figure 11. Map. Close-up of the Amphitheatre Point Landslide reference point.

The lack of stable radar targets identified within close proximity to the Cimarron AOI meant the reference point had to be located nearly 8 km northeast of the landslide. The reference point was selected at a site with relatively flat topography, in a location exhibiting negligible motion over the time period monitored. This point was assumed to be motionless. The reference point location for the Cimarron Landslide is shown in Figure 12. A close up of the reference point is shown in Figure 13. Exact coordinates of the reference point are listed in Table 6.



Figure 12. Map. The location of the Cimarron Landslide reference point.



Figure 13. Map. Close up of the Cimarron Landslide reference point.

DISPLACEMENT RATE

Figure 14 shows the displacement rate of the Permanent Scatterers (PS) and Distributed Scatterers (DS), expressed in mm/yr, identified from the Amphitheatre Point Landslide radar dataset. Figure 15 shows displacement rates for the Cimarron Landslide area. PS/DS are color-coded according to their annual rate of movement. Average displacement values are calculated from a linear regression of the ground movement measured between each consecutive radar image. Detailed information on ground motion is also provided by means of displacement time series, which are provided for each PS and DS.

As discussed in Chapter 2, displacement values are one dimensional. Therefore the movement represented in Figure 14 and Figure 15 indicate ground motion either towards (positive displacement) or away from (negative displacement) the satellites line-of-sight.

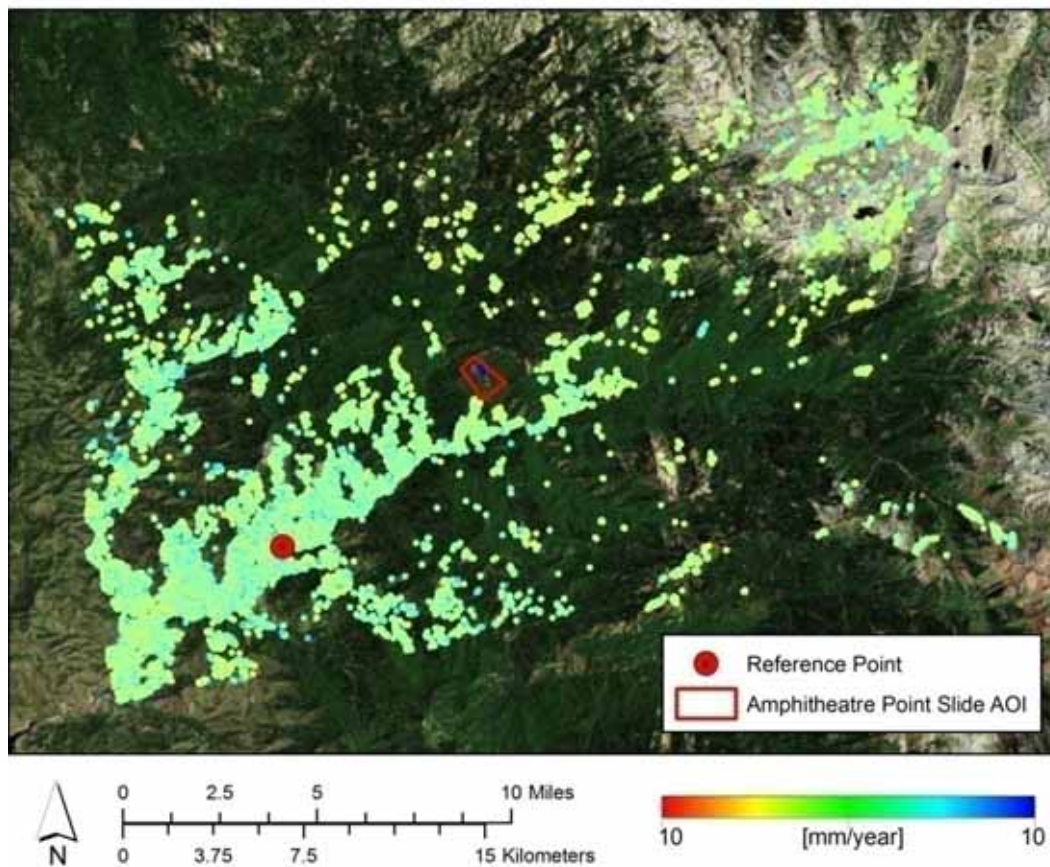


Figure 14. Map. PS and DS displacement rates for the Amphitheatre Point Landslide derived from the SqueeSAR™ analysis.

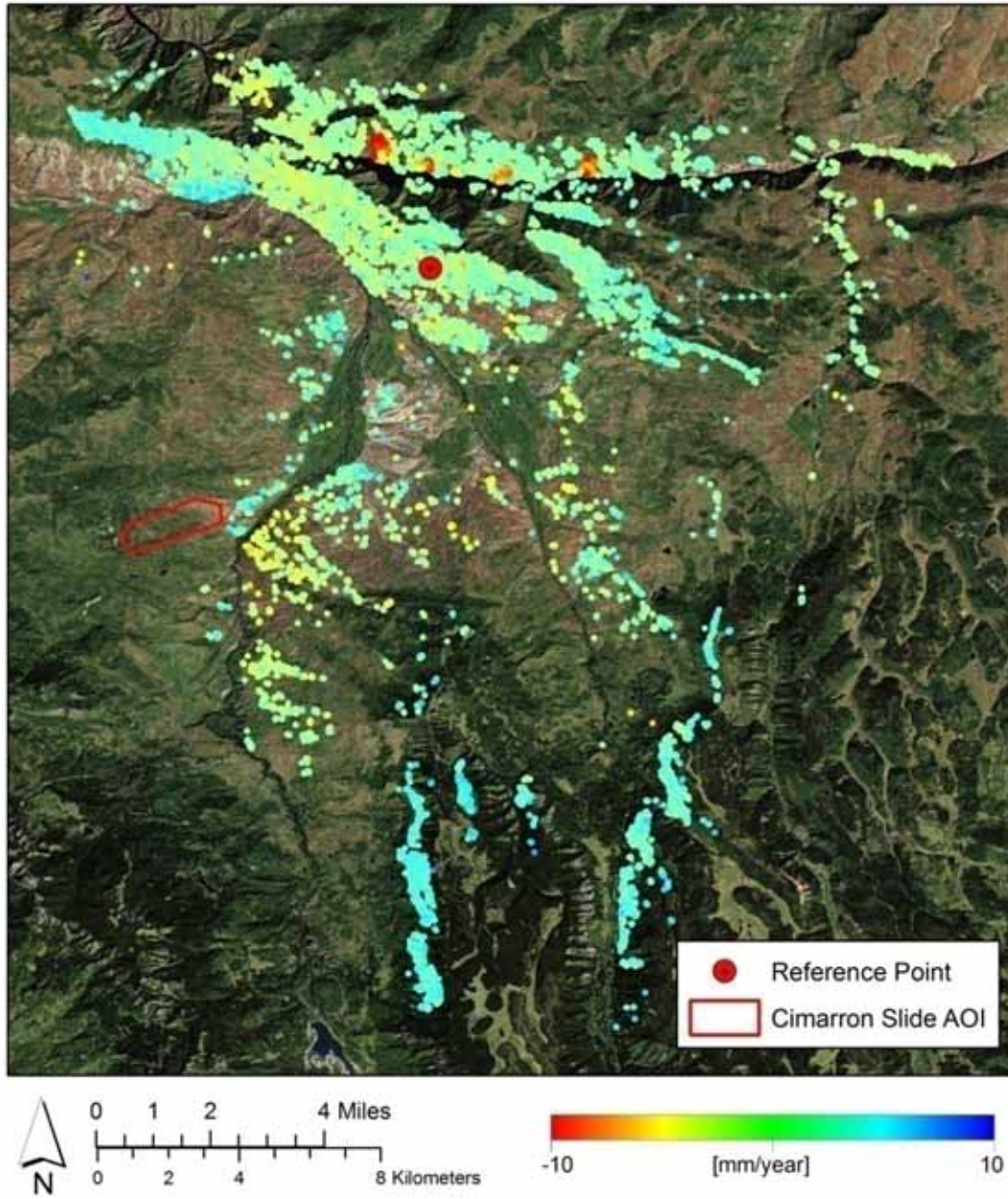


Figure 15. Map. PS and DS displacement rates for the Cimarron Landslide derived from the SqueeSAR™ analysis.

ELEVATION

Figure 16 and Figure 17 show the PS/DS elevation values, in meters, referenced to mean sea level. The elevation value can be used to identify where PS are located. For example, PS on the top of a tower or building will be readily distinguishable from a scatterer at ground level.

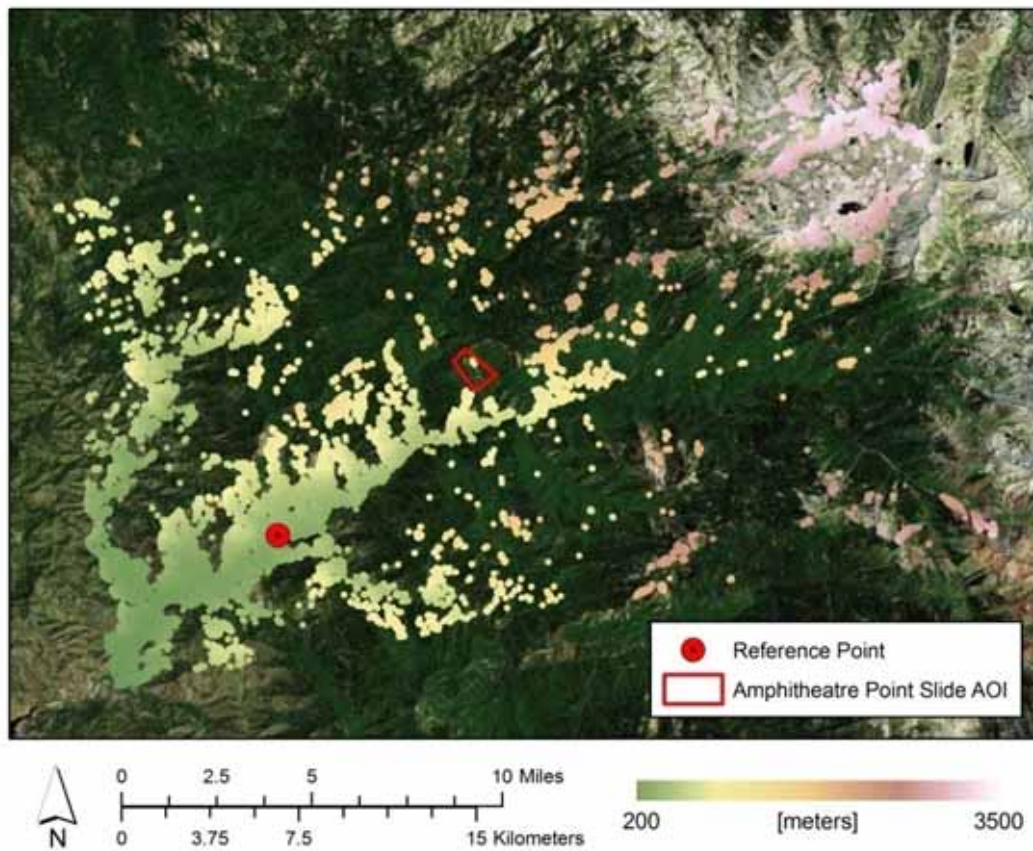


Figure 16. Map. PS and DS elevation for the Amphitheatre Point Landslide, displayed in meters above sea level.

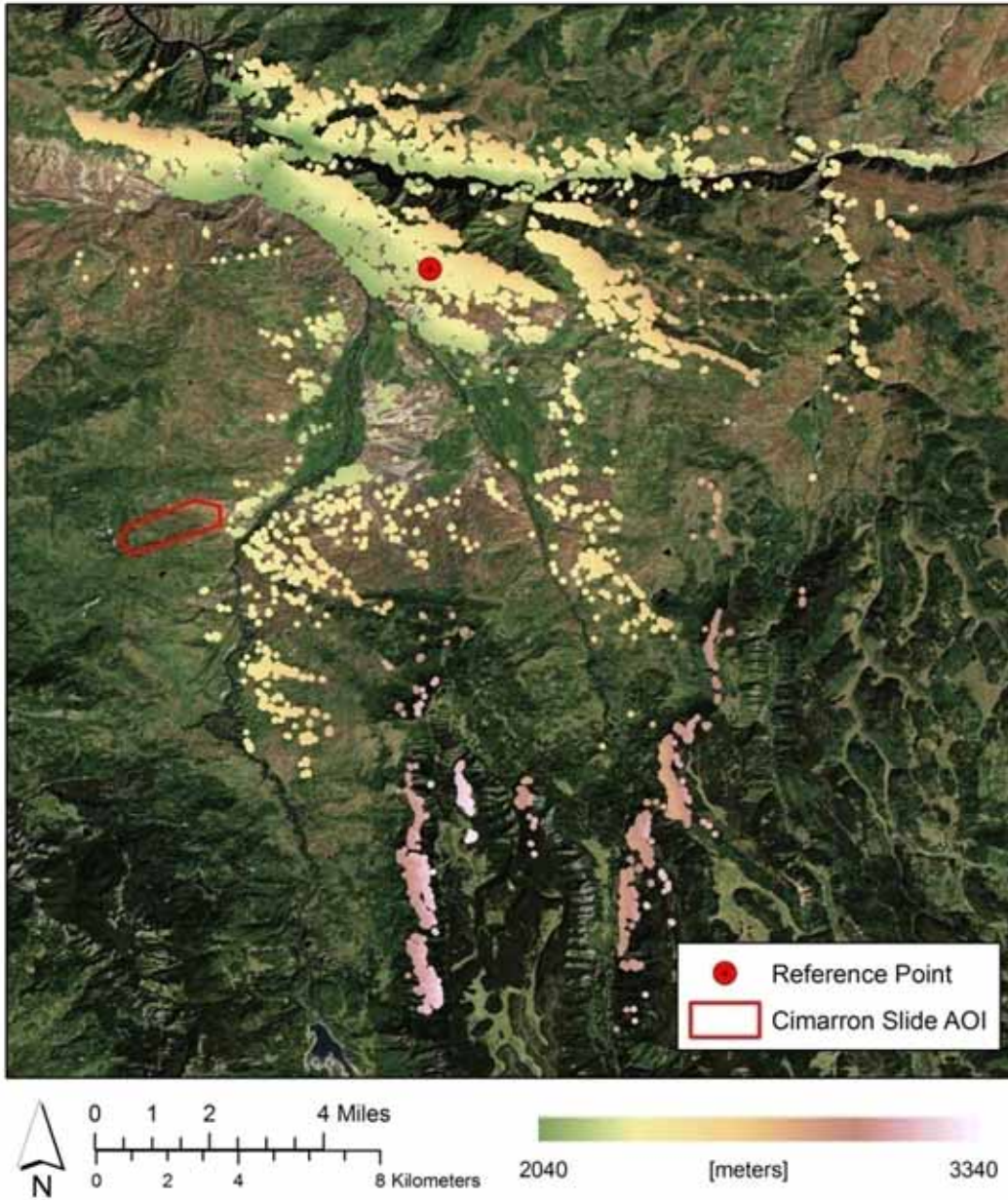


Figure 17. Map. PS and DS elevation for the Cimarron Landslide, displayed in meters above sea level.

ACCELERATION

PS/DS acceleration values like those in Figure 18 and Figure 19 can be used to identify non-linear trends in the time series. Negative accelerations are marked in red and indicate either an increase in downward movement rates or a decrease in upward movement rate. Positive accelerations are blue and indicate either an increase in the rate of uplift or a decrease in the rate of subsidence.

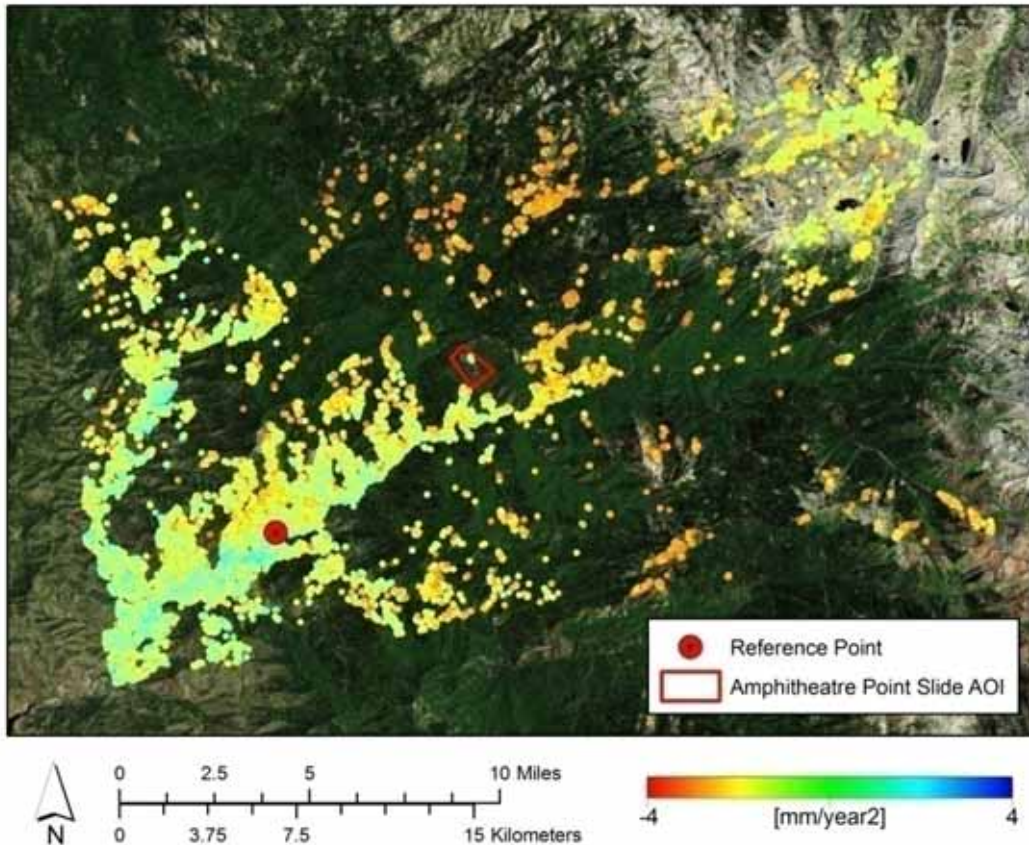


Figure 18. Map. PS and DS acceleration for the Amphitheatre Point Landslide, in mm/yr².

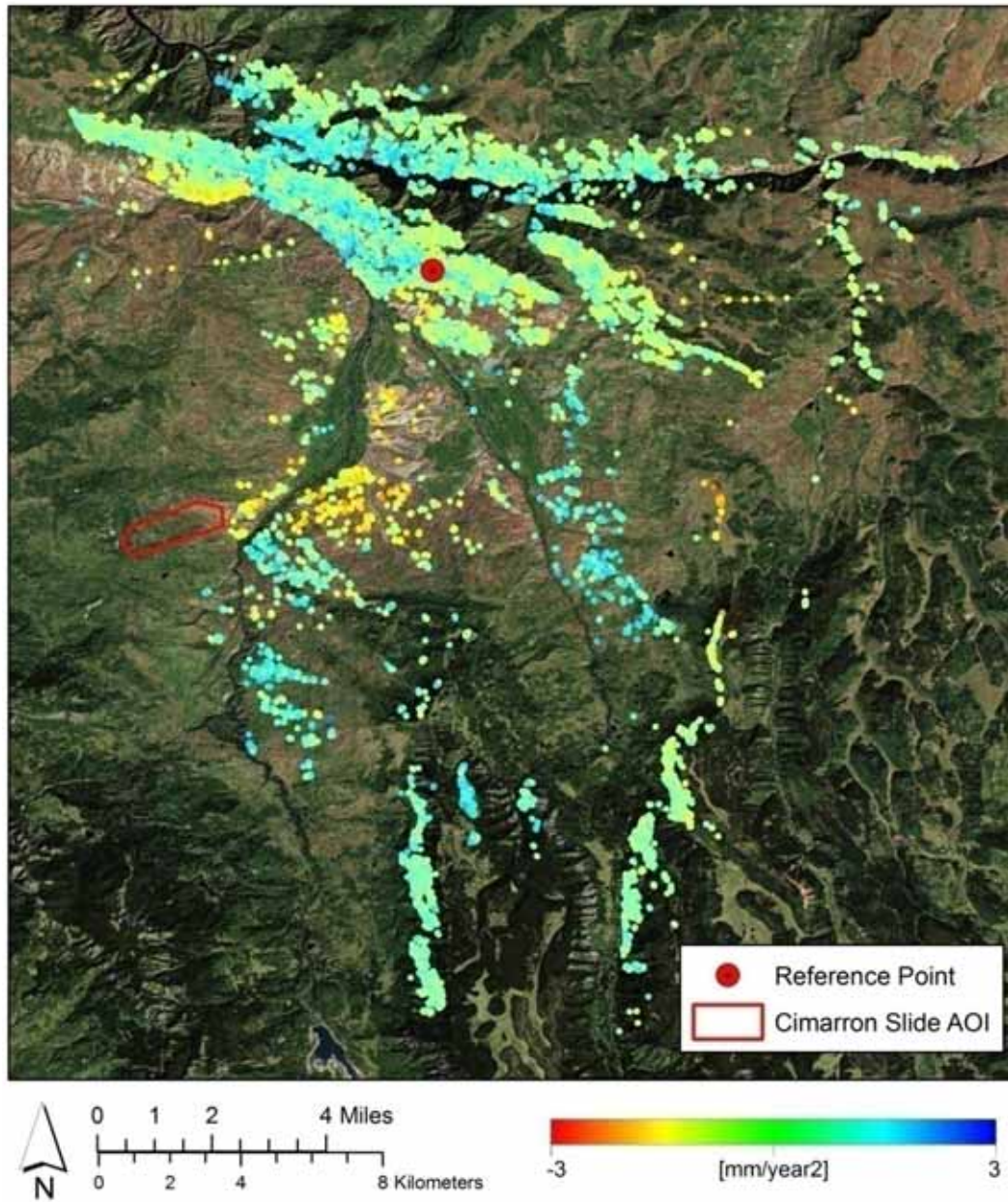


Figure 19. Map. PS and DS acceleration for the Cimarron Landslide, in mm/yr^2 .

OTHER PROPERTIES OF THE DATA

Table 5, below, provides a summary of the other properties relative to processing the Amphitheatre Point Landslide data. Table 6 summarizes the properties of the Cimarron Landslide data processing.

Table 5. Statistics of the processed Amphitheatre Point Landslide data.

Satellite	ENVISAT-2
Acquisition geometry	Ascending
Critical baseline [m]	1095.80
Analysis time interval	10/29/2003- 2/24/2010
Number of scenes processed	40
Georeferencing	PS aligned on Microsoft Virtual Earth (Bing Maps)
Projection system used / datum	GCS_WGS_1984
Reference Point location	LAT: 36.4759, LONG: -118.8558
Area of interest	0.459 mi ² (1.19 km ²)
Size of entire area processed	238.67 mi ² (618.15 km ²)
Number of PS + DS identified within the AOI	5
- Number of PS	3
- Number of DS	2
Number of PS + DS identified within the entire area processed	37,143
- Number of PS	1,797
- Number of DS	35,346
Average PS + DS density within entire area processed	156 PS/DS per mi ² (60 PS/DS per km ²)

Table 6. Statistics of the processed Cimarron Landslide data.

Satellite	RADARSAT-1
Acquisition geometry	Descending
Critical baseline [m]	5038.44
Analysis time interval	12/29/2003 - 3/27/2010
Number of scenes processed	30
Georeferencing	PS aligned on Microsoft Virtual Earth (Bing Maps)
Projection system used / datum	GCS_WGS_1984
Reference Point location	LAT: 38.423, LONG: -107.5132
Area of interest	0.683 mi ² (1.77 km ²)
Size of entire area processed	136.073 mi ² (352.43 km ²)
Number of PS + DS identified within the entire area processed	35,514
- Number of PS	1,219
- Number of DS	34,295
Average PS + DS density within entire area processed	261 PS/DS per mi ² (101 PS/DS per km ²)

The critical baseline is the maximum admissible separation distance between satellite orbits for an InSAR analysis. Interferometry cannot be performed if the orbits are separated by more than this distance.

CHAPTER 4 – OBSERVATIONS

TARGET DISTRIBUTION AND DENSITY

Amphitheatre Point

Radar target densities achieved from the SqueeSARTM processing of the entire Amphitheatre Point satellite image were 156 PS/DS per mi² (60 PS/DS per km²). These values are fairly high considering the challenging characteristics of this area for the application of InSAR.

Despite the good density of radar targets, the spatial distribution of the PS/DS points was highly irregular, as Figure 14 showed earlier. Many of the highest densities of PS/DS points throughout the entire extent were identified in areas with little to no vegetation and were clustered around the Kaweah River, which can be seen in the southern half of Figure 10 shown earlier. PS/DS distributions are especially dense along the river where the surrounding terrain is relatively level, and in the communities of Three Rivers and Kaweah, CA.

Radar target identification was limited within the AOI for three main reasons:

- decorrelation of the radar data due to dense vegetation;
- the use archive radar imagery; and
- geometric errors in the radar imagery due to the topography of the area.

Each of these points is discussed in greater detail below.

First, the identification of measurement points was unsuccessful over any portion of the AOI covered by dense vegetation. Radar targets (PS and DS) can only be extracted from stable areas with relatively consistent reflectivity patterns over time. As shown earlier in Figure 4, vegetation appears to cover approximately two-thirds of the entire AOI, significantly limiting the area from which radar targets could be identified.

Second, as the objective of this project was to measure historic ground movement, the radar data used in this analysis was limited to pre-existing archive imagery. While the most complete archive dataset available was used to analyze this area, there is no control over the acquisition parameters used to capture this radar dataset. As a result, the orbital geometry of the satellite was not optimized for this site, increasing the degree to which geometric errors impeded site visibility.

Third, the topography of the Amphitheatre Point AOI is very steep, meaning portions of this area are subject to geometric errors. As all radar imagery is acquired from a right-looking, off-nadir angle, areas with steep slope gradients can appear distorted (or can be blocked completely) in the satellites field of view. These areas of distortion represent geometric errors, which can be identified in Figure 20 from an amplitude map of the area. Amplitude values represent the amount of radiation backscattered to the satellite by features on the ground. Areas that appear to be white or light gray often represent geometric errors, meaning no radar targets can be identified from these areas.

In contrast, darker areas (dark gray or black) represent amplitude values for areas not as likely to be affected by geometric errors. Low amplitude values are most often recorded over exposed environments (such as bare ground and sparsely vegetated land) or areas with an abundance of man-made structures (such as towns or cities). As shown in the bottom panel of Figure 20, radar targets are often identified from areas that appear dark gray.

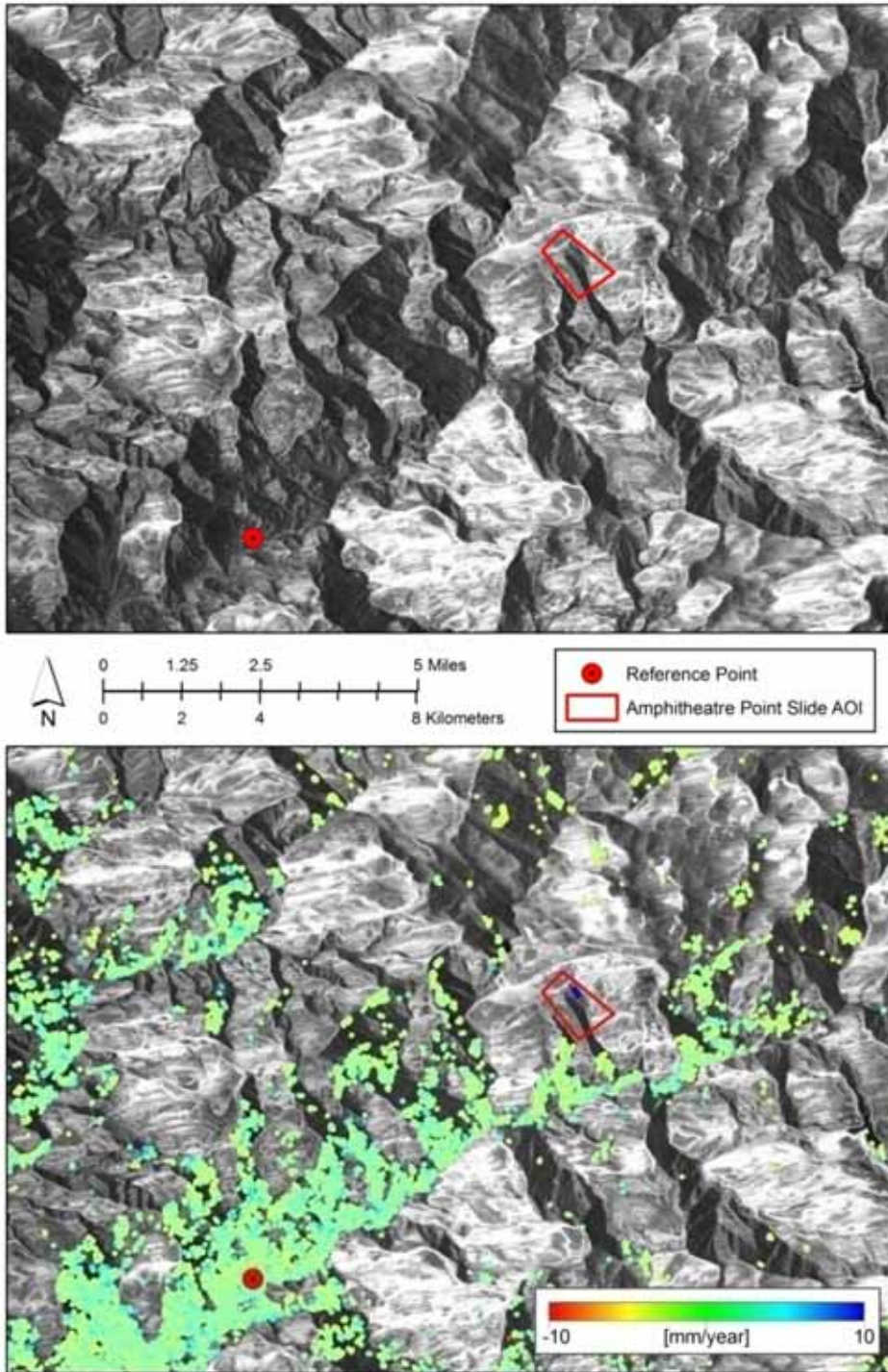


Figure 20. Map. Amplitude map (top panel) and an amplitude map with all identified PS and DS targets colored by displacement rates (bottom panel) shown for the area surrounding the Amphitheatre Point Landslide.

Figure 21 shows amplitude values for the AOI. Over half of the area within the AOI (light gray or white) is obstructed by geometric errors, and therefore would not possess radar targets even in the event of ideal surface conditions. The lack of radar targets in dark gray or black areas is likely due to interference caused by vegetation coverage.

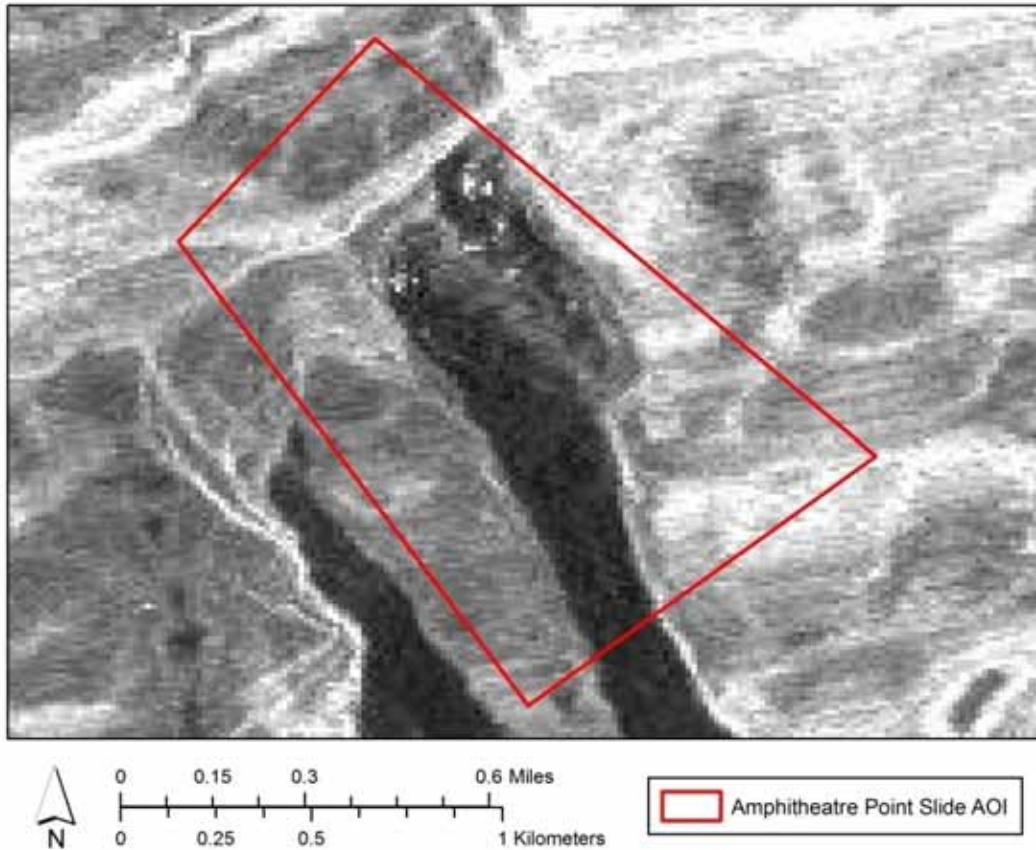


Figure 21. Map. Close-up of the amplitude map over the Amphitheatre Point Landslide AOI.

Cimarron

The density of radar targets identified throughout the entire Cimarron area processed with the SqueeSARTM algorithm was 261 PS/DS per mi² (101 PS/DS per km²). This density is fairly high, which was expected given the previous success of this approach in similar environments. However, no points were identified within the AOI.

The spatial distribution of the PS/DS points was highly variable throughout the extent of the satellite image as Figure 15 showed earlier. The highest radar target densities were found in the northern portion of the radar scene, clustered around a reservoir. High densities were also achieved over areas with little vegetation cover or exposed ground. In contrast, very few points were identified in vegetated areas, which are predominant in the southern portion of the entire area analyzed, and within the AOI extent. Vegetation exhibits significant variability over time, causing decorrelation in the radar data and preventing PS and DS identification.

While the presence of vegetation is thought to be the primary cause for the lack of radar targets in the AOI, snow cover may also be an impediment. The presence of snow in radar scenes acquired during winter months can also cause radar data to decorrelate. As the AOI is located at a slightly higher elevation than many other areas in the satellite image extent, it is possible that snow cover may also have been a contributing cause in the lack of data point.

Another common factor impeding PS/DS identification, are geometric errors caused by unsuitable satellite acquisition parameters. However, such errors are normally expected in radar images captured over areas of steep topography. In the case of the Cimarron Landslide, the low gradient of the slopes at this location means unsuitable acquisition geometry is not a likely cause of unsuccessful InSAR analysis. An amplitude map (representing the amount of radiation backscattered to the satellite by features on the ground) of the area indicates that geometric errors were likely not a predominant factor preventing radar target extraction over the AOI as shown in Figure 22. Areas impacted by geometric errors often appear white or light gray in amplitude scenes.

Figure 23 shows amplitude values for the AOI. Few areas of geometric errors (white or light gray) are obvious within this area.

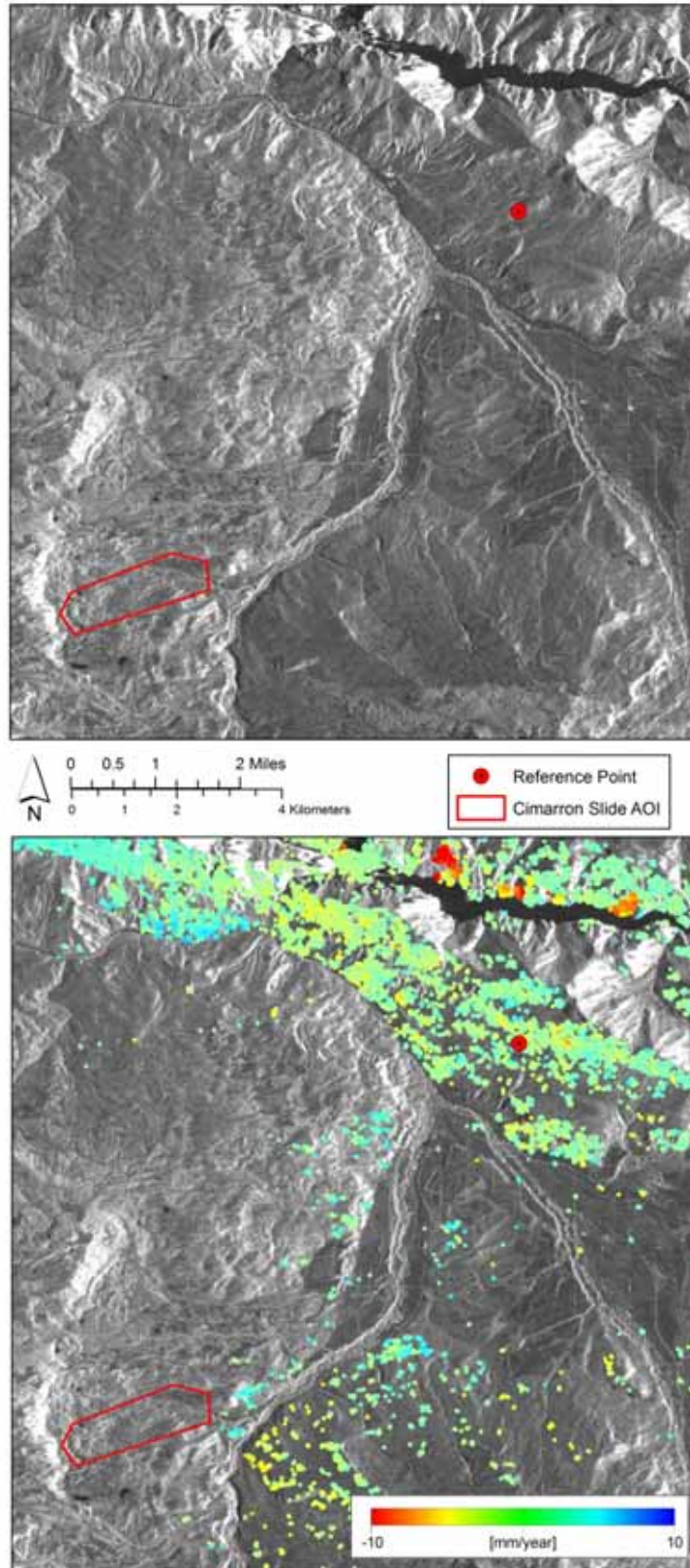


Figure 22. Map. Amplitude map (top panel) and an amplitude map with all identified PS and DS targets coloured by displacement rates (bottom panel) shown for the area surrounding the Cimarron Landslide.

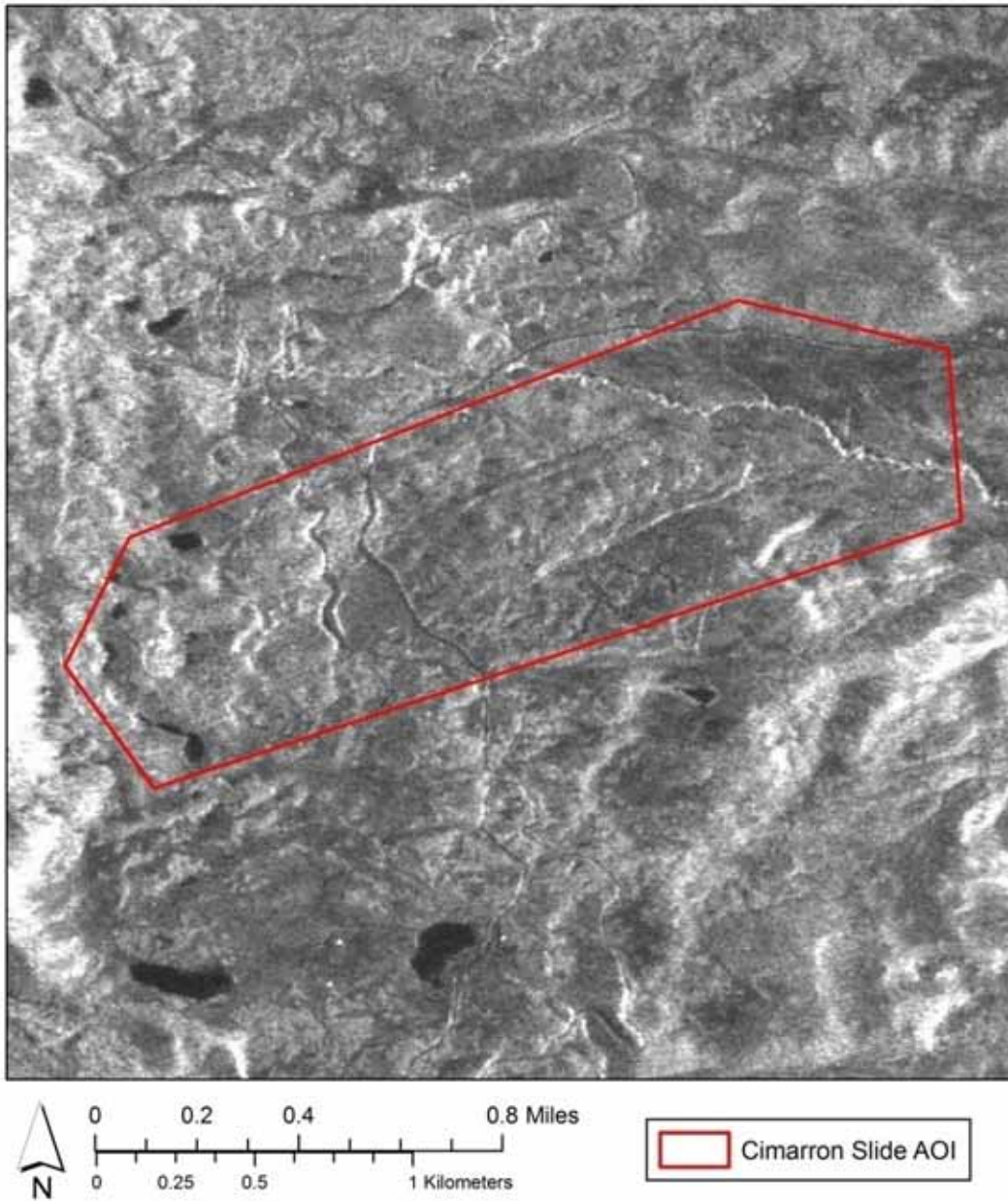


Figure 23. Map. Close-up of the amplitude map over the Cimarron Landslide AOI.

LANDSLIDE MOVEMENT

Amphitheatre Point

Despite the significant challenges of this site for InSAR applications, a cluster of radar targets was identified within the Amphitheatre Point AOI as shown in Figure 24. This cluster consisted of a small group of highly consistent and coherent (stable) PS and DS points. It should be noted that while this group of radar targets is included based on their high coherence and consistency, the movement associated with these points could be the result of phase unwrapping errors and therefore, not necessarily representative of actual ground displacement.

The results shown earlier in Figure 14 represent 1-Dimensional line-of-sight (LOS) data, meaning all movement is observed relative to the position of the satellite. As a result, any displacement measured by a PS or DS includes motion occurring in both vertical and horizontal (east-west and north-south) directions. In cases of complex movement (such as landslides), motion is often 3-Dimensional, which is not easily represented using a single acquisition geometry and often complicates interpretation of the results.

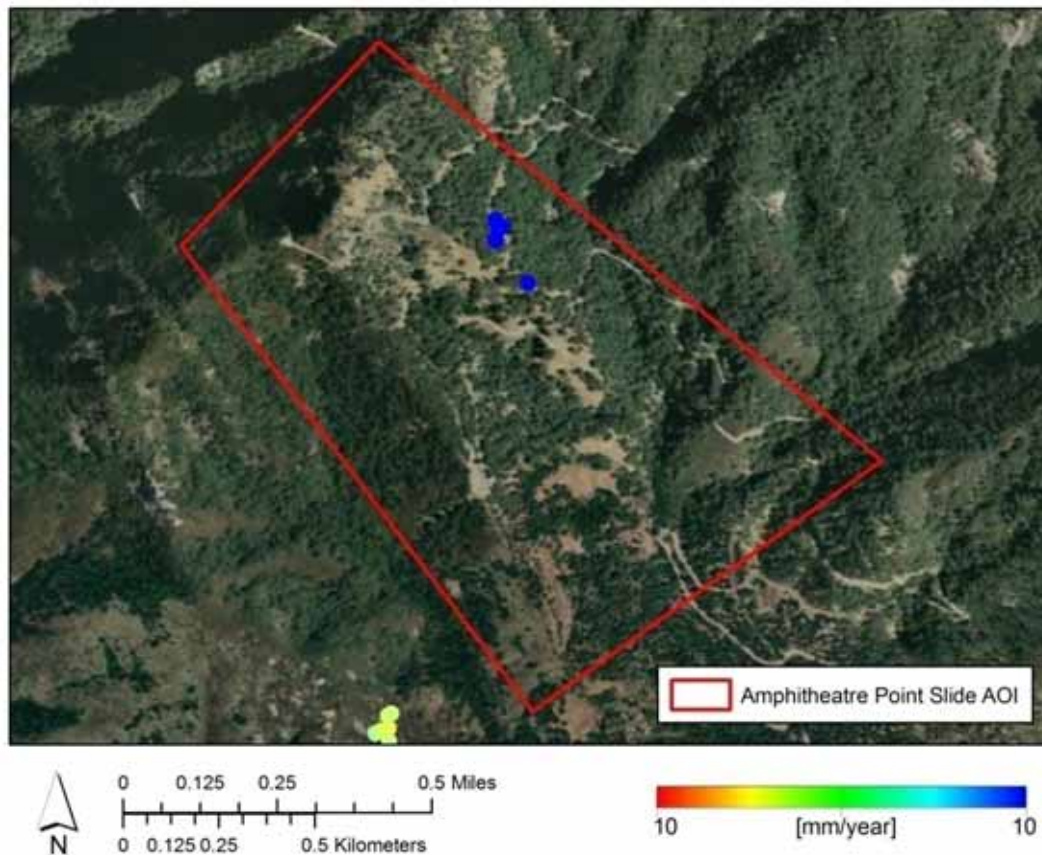


Figure 24. Map. PS and DS displacement rates derived from the SqueeSAR™ analysis shown for the Amphitheatre Point Landslide AOI.

As the radar dataset used in this analysis was captured from a satellite travelling from south to north and imaging to the east, the positive displacement values could be interpreted as western motion (horizontal movement towards the satellite). However, due to the spatial isolation of these data points, further validation of the displacement observed at these radar targets is required before this conclusion can be reached. Verification of these results is also important given the somewhat uncharacteristic behavior of the PS and DS and the uncertainty noted above, and would be required in order to eliminate the possibility of a radar interpretation error during data processing. The maximum likelihood method was used for result validation.

MAXIMUM LIKELIHOOD RESULTS

While interpretation of ground movement from the ML results is somewhat challenging, this approach does provide a general indication of ground movement occurring over a local area. Figure 25 shows results for the Amphitheatre Point area. Figure 26 shows results for the Cimarron area.

It should be emphasized that the ML results used the interferogram with the highest coherence, or quality, out of a possible 780 for the ERS dataset obtained over the Amphitheatre Point Landslide (the number of possible pairs within a dataset containing 40 images) and a possible 435 for the RADARSAT dataset over the Cimarron Landslide (the number of possible pairs within a dataset containing 30 images) to represent ground movement.

Areas that appear to be homogeneous in color (bottom panel of Figure 25 and Figure 26) indicate areas with high coherence. In general, areas over which SqueeSAR™ points were identified correspond well to areas identified as coherent from the ML analysis. In general, these homogeneous (coherent) areas provide reliable measurements of displacement.

The results of the ML analysis over the Amphitheatre Point Landslide allow for two important observations to be made. First, the adverse environmental characteristics of the Amphitheatre Point Landslide AOI render most of the site unsuitable for the application of InSAR. As seen in Figure 25, even a pixel by pixel compilation of the most coherent interferograms over this site indicates the area is too decorrelated for InSAR analysis. Second, by comparing the results of the SqueeSAR™ analysis with the outcome of the ML approach, it is likely that the magnitude of movement measured by the small cluster of radar targets identified with the SqueeSAR™ algorithm is incorrect. Based on the ML results, it appears as though little to no movement is occurring within the small area of coherence within the AOI as Figure 25 shows.

The inaccurate displacement values attributed to the PS and DS identified in the Amphitheatre Point area are most likely caused by phase unwrapping errors. Phase unwrapping is the procedure used to translate shifts in the radar signal into ground deformation values. Errors in the phase unwrapping process occur when the direction of ground movement for a given area is misinterpreted.

The results of the ML analysis over the Cimarron Landslide indicate that the radar data acquired over this site is completely decorrelated, even with the use of the most coherent data available from the entire radar dataset as Figure 26 shows. Several coherent areas can be identified in close proximity to the toe of the slide; however no significant ground displacement was observed from

the results. Despite the inability of the ML approach to extract additional information over the Cimarron Landslide, this technique was capable of increasing the coverage of deformation data in the surrounding area, particularly to the east of the AOI.

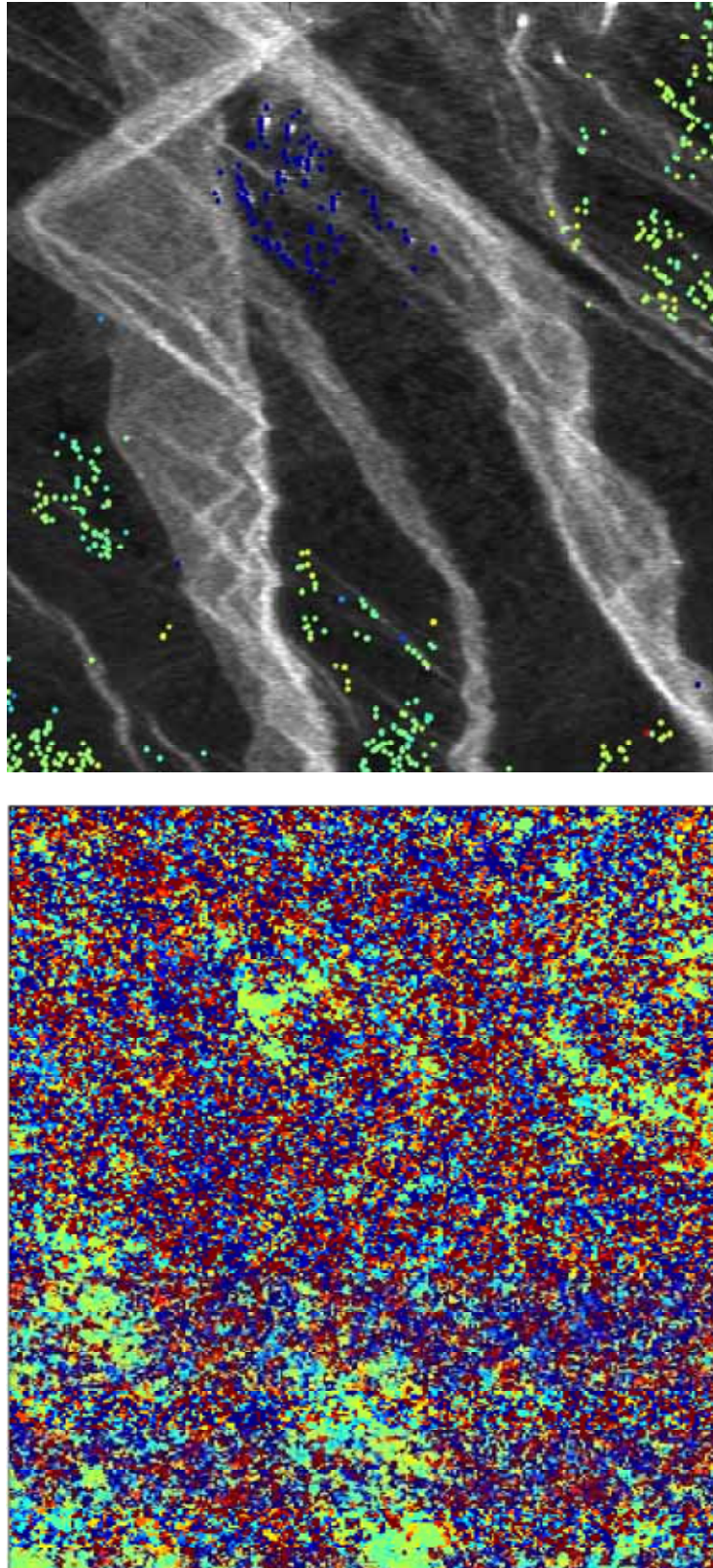


Figure 25. Map. Results of the SqueeSAR™ analysis (prior to data filtering for quality control) for the area surrounding the Amphitheatre Point Landslide AOI (top panel) and results of the Maximum Likelihood analysis for the same spatial extent.

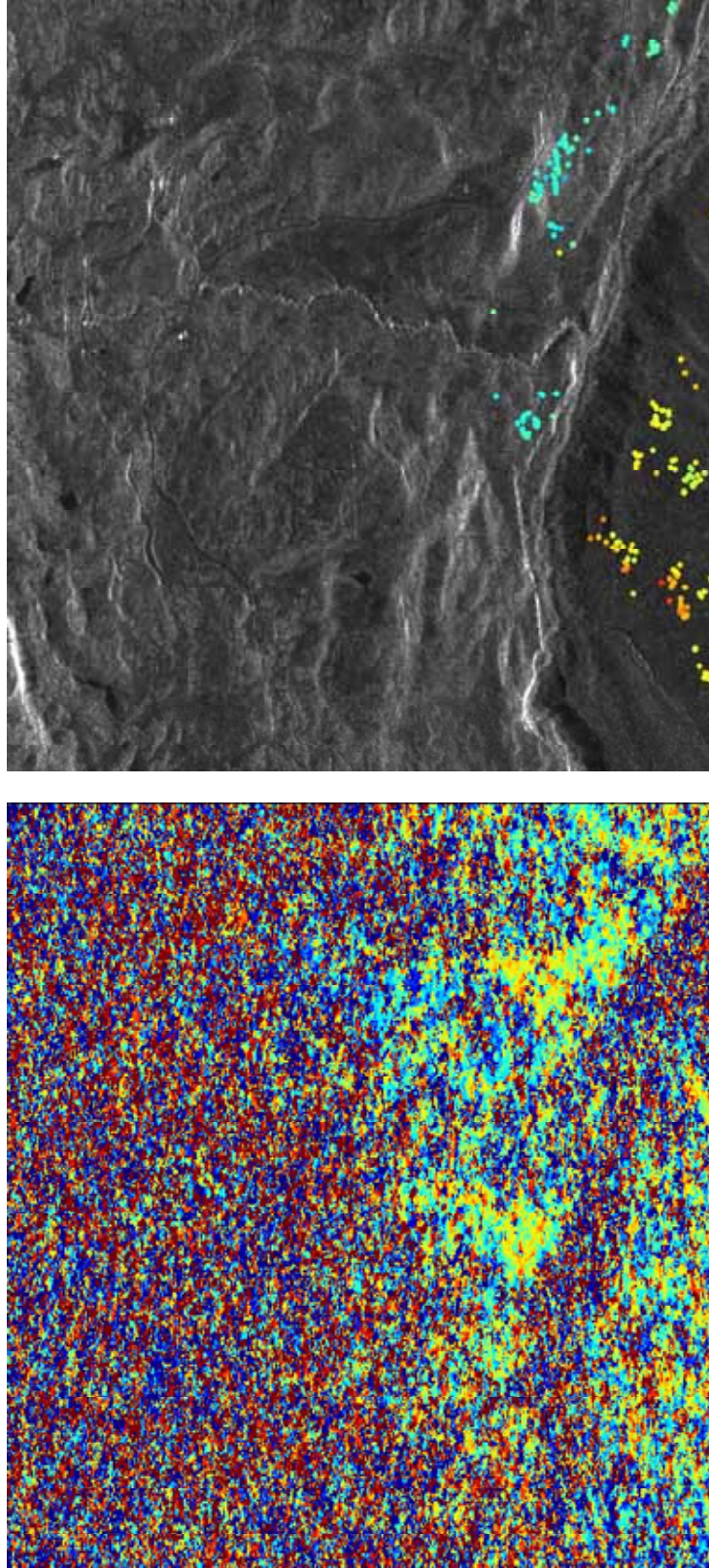


Figure 26. Map. Results of the SqueeSAR™ analysis (prior to data filtering for quality control) for the area surrounding the Cimarron Landslide AOI (top panel) and results of the Maximum Likelihood analysis for the same spatial extent.

ADDITIONAL OBSERVATIONS

Cimarron

Despite the lack of PS and DS points identified at the Cimarron site, several additional landslides were identified outside the AOI, at the northern region of the satellite image as Figure 15 showed earlier. Figure 27 shows SqueeSAR™ results for two of the westernmost landslides visible in this additional cluster. The high density of radar targets at this location allow for the successful demonstration of this technique for identifying landslide activity. As seen in Figure 27, the footprints of two distinct landslides are clearly visible within the PS and DS points. Furthermore, all points identified in these landslides are highly coherent and measure significant downward movement. The lack of vegetation at this location is likely the primary reason the SqueeSAR™ algorithm was successful.

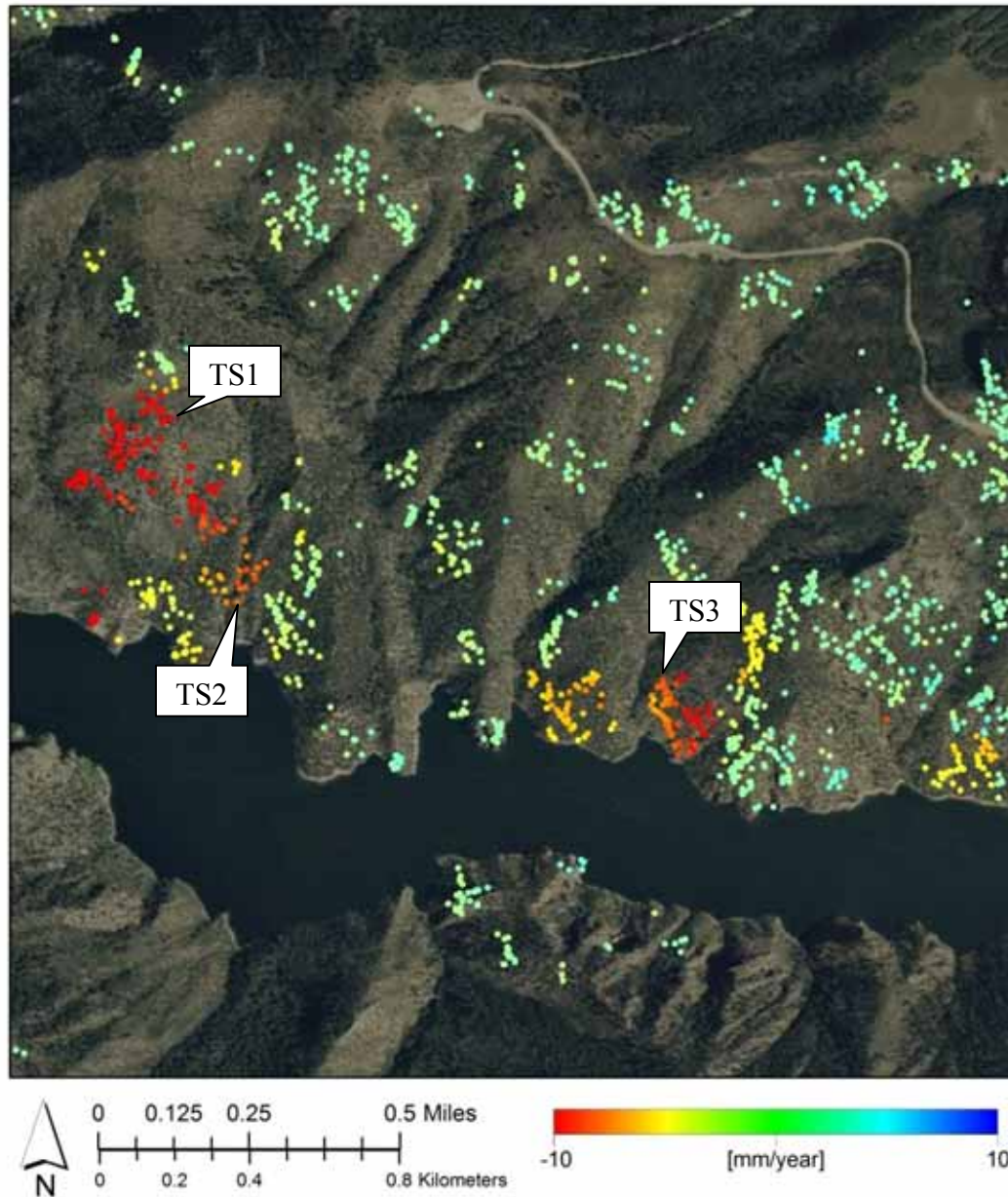


Figure 27. Map. PS and DS displacement rates derived from the SqueeSAR™ analysis shown for several landslides identified in the north portion of the radar scenes processed.

The observation and analysis of time series data can provide a wealth of additional information on the behaviour of each PS/DS that sometimes cannot be obtained by observing only the mean deformation rate of an area. Figure 28, Figure 29 and Figure 30 show time series data for three radar targets identified within these additional landslides. Significant downward motion (motion away from the satellites line of site) can be observed at each of these points.

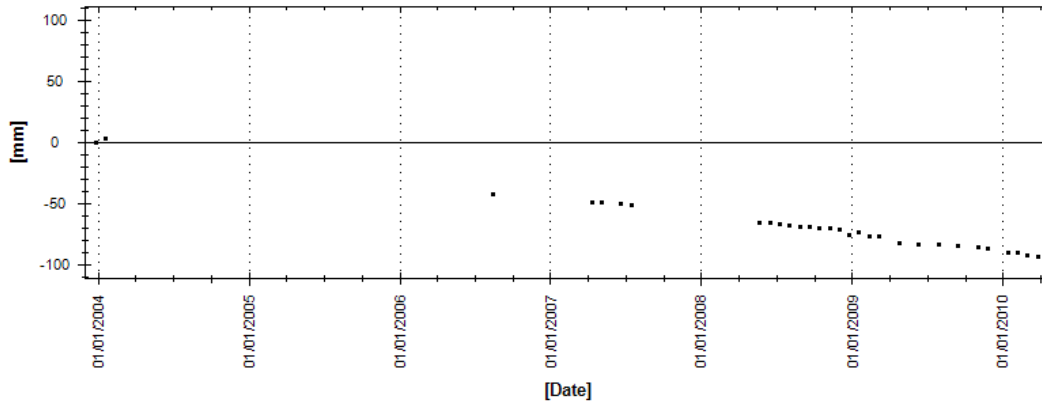


Figure 28. Graph. Time series for the point labeled TS1 in Figure 27.

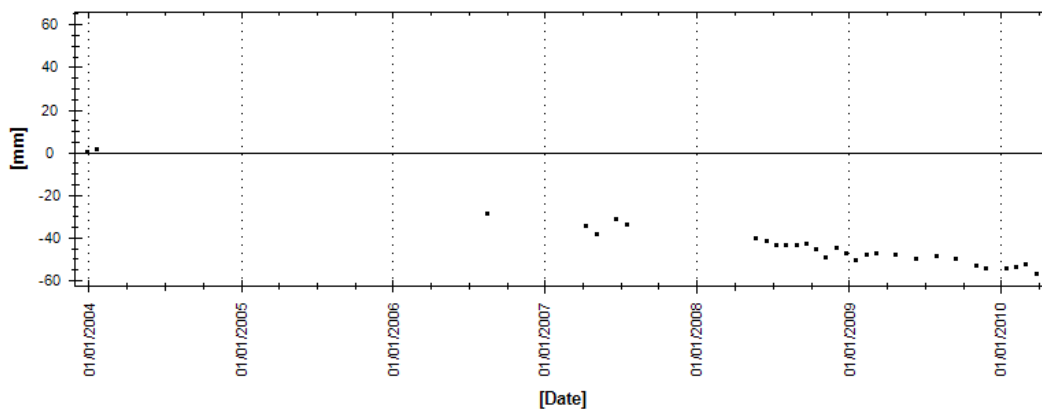


Figure 29. Graph. Time series for the point labeled TS2 in Figure 27.

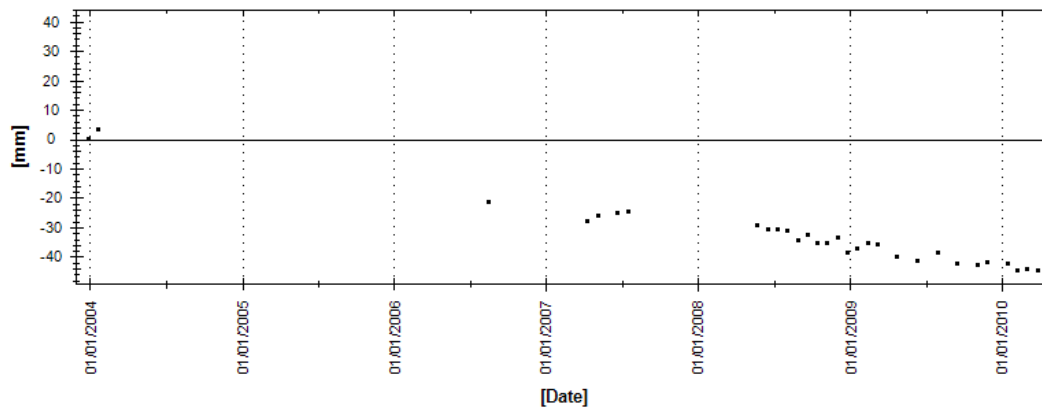


Figure 30. Graph. Time series for the point labeled TS3 in Figure 27.

CHAPTER 5 – PRECISION ASSESSMENT

GENERAL

Three parameters are used to characterize the PS results:

- Precision of the estimated displacement results;
- Precision of the estimated elevations;
- Precision of the geocoding.

The typical precision of measured displacement rates obtained from the SqueeSAR™ analyses of Envisat satellite imagery is <1 mm/yr for all radar targets located within 1 km of the reference point and estimated from a dataset containing 45 SAR acquisitions or more. If a single displacement value (displacement between contiguous satellite images) is considered, the accuracy decreases slightly to 5 mm, provided the radar target is located within 1 km from the reference point and processed using a dataset containing more than 45 scenes.

While the Amphitheatre Point AOI is approximately 10 km away from the reference point, the accuracy of the results is still expected to be fairly high given the high number of scenes used for this analysis (40), the high coherence of the data (as shown in Appendix B) and the low standard deviations of the measurement points.

As no measurement points were identified within the Cimarron AOI, the accuracy of the results with regard to the objectives of this project cannot be reported. However, the accuracy of ground displacement estimated throughout the remainder of the satellite image is expected to be fairly high given the high coherence of the data (as shown in Appendix B) and the low standard deviations of the measurement points.

Positional (elevation and geocoding) errors are determined by the resolution of the SAR system in use. The Envisat satellite has a cell size of 20 m in the *range* direction (east-west) and 4 m in the *azimuth* direction (north-south direction). The RADARSAT-1 satellite has a cell size of 20 m in the *range* direction (east-west) and 5 m in the *azimuth* direction (north-south). For data of this resolution, geocoding accuracy generally equals ± 6 m in *range* direction, ± 2 m in *azimuth* direction and ± 1.5 m in elevation (height) for all points located within 1 km of the reference point and estimated from a dataset with at least 45 scenes.

PRECISION OF THE RESULTS

The most important factors impacting data precision are:

- Spatial density of the PS (the lower the density, the higher the error)
- Quality of the radar targets (signal-to-noise ratio levels)
- Climatic conditions at the time of the acquisitions
- Distance between the measurement point and the reference

The precision of the Amphitheatre Point data (one standard deviation) is shown in Figure 31. Precision of the Cimarron results are shown in Figure 32. Standard deviation values of the estimated displacement rates are a function of the factors listed above and of local ground movement dynamics.

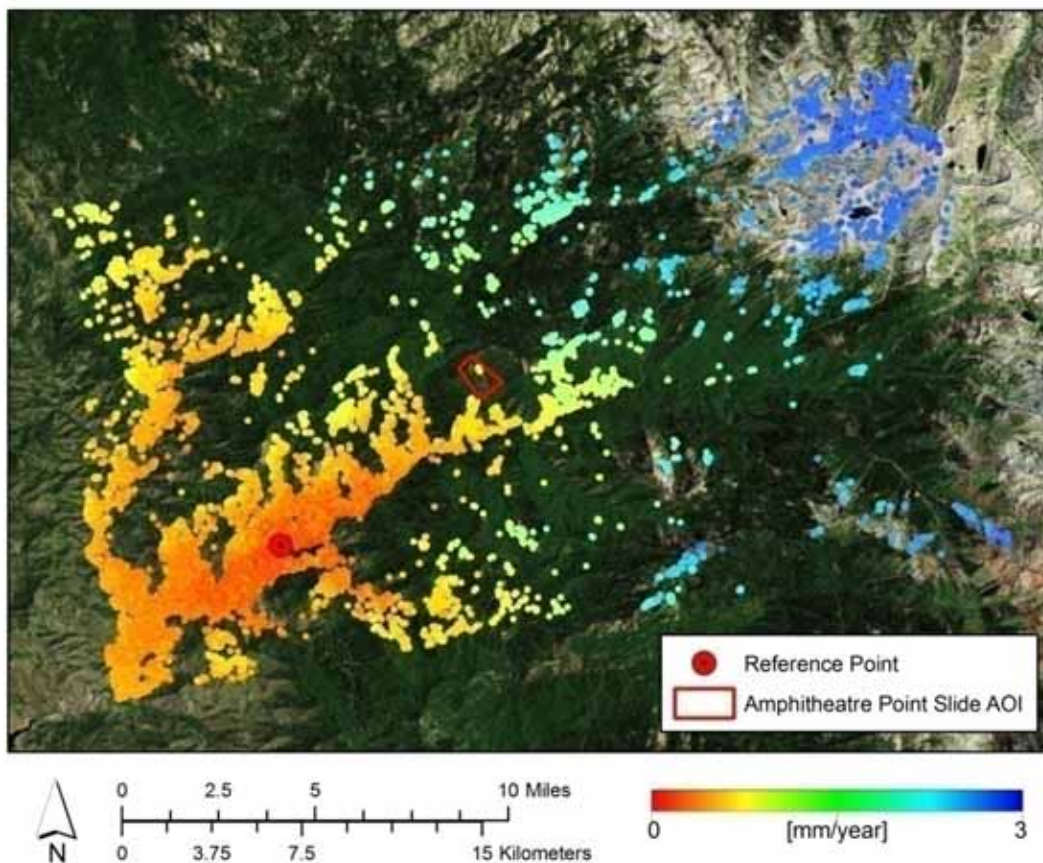


Figure 31. Map. Standard deviation of the displacement rates estimated from the SqueeSAR™ data over the Amphitheatre Point Landslide area.

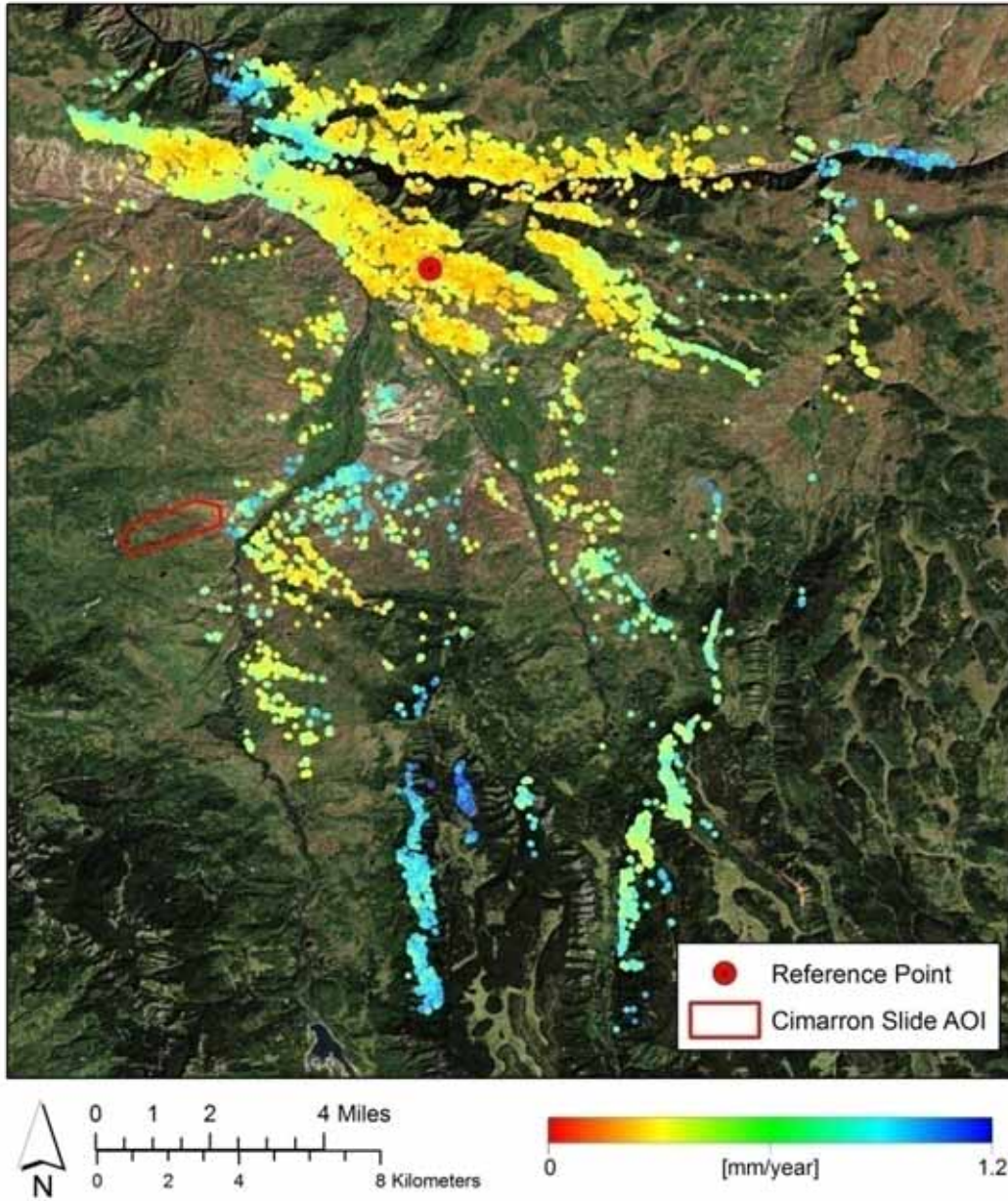


Figure 32. Map. Standard deviation of the displacement rates estimated from the SqueeSAR™ data over the Cimarron Landslide area.

CHAPTER 6 – CONCLUSIONS

SqueeSAR study conclusions are presented below. In addition, results from conventional InSAR previously performed at the Cimarron site (2006) and Amphitheatre site (2009) are presented here for reference. More detailed discussion of these latter activities is available in the original documents.

AMPHITHEATRE POINT

SqueeSAR

The application of SqueeSAR™ to the Amphitheatre Point Landslide was largely unsuccessful. While a small cluster of points was identified using this approach, a secondary analysis (the Maximum Likelihood analysis) found that the displacement rates measured over these areas were not completely reliable. As a result, while several stable radar points were extracted over the body of the landslide, there is a limited confidence associated with their interpreted displacement rates.

It is important to highlight that in other areas of the satellite image covering the Amphitheatre Point Landslide AOI, the SqueeSAR™ algorithm was highly successful in extracting a good density of PS and DS points. For instance, numerous PS and DS points were identified in areas with sparse vegetation coverage, rocky surfaces or man-made structures as Figure 14 showed earlier. In order to better demonstrate the SqueeSAR™ technique, the results of the analysis over the full satellite scene are included in this report, and not just the area covered by the Amphitheatre Point Landslide.

The ML approach was also performed over the Amphitheatre Point Landslide in an attempt to extract more information from the area. Minimal gains in displacement information were achieved using this technique and did not produce results for any additional areas within the AOI.

InSAR

Four data RADARSAT-1 satellite sets were available in 2007 after installation of the three corner Reflectors (CR) for measuring the deformation. Deformation at the CRs was reliably measured. The CRs appeared as bright dots in the radar imagery and were very visible. The noise of the deformation measurements was at the millimeter level, which was apparent from the smoothness of the deformation profile. The measured deformation had a magnitude and direction (down the slope) that appeared very reasonable. The limiting factor in the accurate of the measurements was because of uncertainty of the heights of the installed CRs. The height was not measured during installation and the USGS 10 m DEM was used to obtain the height using bilinear interpolation at the provided position. The deformation measurements were estimated to have a precision of approximately 0.9 mm.

The following observations were made:

- The CRs were well-installed and successful precise deformation measurements were made. ▪ CR#2 showed a local downslope movement of 3.43 mm (flow-line deformation) compared to CR#1 over the same time period (September 25, 2007 to December 30, 2007).

- CR#3 showed a local downslope movement of 2.32 mm (flow-line deformation) compared to CR#1 over the same time period (September 25, 2007 to December 30, 2007).

Two conventional deformation maps were produced from this study. Unfortunately, temporal decorrelation was significant which made it impossible to generate coherent radar interferograms at any time period for this location. Nonetheless, the maps provided some information on the deformation that occurred in the observed time frames.

- Pair A for the time period August 8, 2007 to October 19, 2007 (72 days). ~4 mm of deformation measured in the area with a precision of ~7 mm.
- Pair B for the time period December 6, 2007 to December 30, 2007 (24 days). ~6 mm of deformation measured with a precision of ~5 mm.

Masked out areas due to temporal de-correlation were large. No large deformation phenomena were observed in these deformation maps.

CIMARRON

SqueeSAR

Due to the adverse environmental conditions at the Cimarron AOI, the application of the SqueeSAR™ algorithm was not a success. While several points were identified to the east (down slope) of the landslide, displacement measured at these areas indicated that no significant ground movement had occurred over the time period analyzed. This observation was confirmed using a secondary InSAR approach (the Maximum Likelihood analysis). Overall, since no stable points could be extracted over the area of interest, no conclusions can be drawn as to the nature of the ground movement occurring at this location.

Again, it should be highlighted that in other areas of the satellite image, the SqueeSAR™ algorithm was highly successful in extracting a good density of PS and DS points, particularly in areas with sparse vegetation coverage or exposed ground as Figure 15 showed earlier. Similar to the Amphitheatre Point Landslide analysis, the results of the analysis over the full satellite scene are included in this report, and not just the area covered by the Cimarron Landslide.

It is also worth emphasizing the successful identification and measurement of several landslides outside of the AOI. These additional landslides were detected due to the abundance of stable (coherent) radar targets extracted from this portion of the satellite image. Significant downward motion was observed for at least four different landslides at this location.

InSAR

In this location, there are 11 ERS-1 images from 1992 to 1996, and a further 37 ERS-2 images between 1995 and 2001. As part of ERS image selection, precipitation and temperature information were gathered to allow the selection of scenes acquired outside of precipitation periods or when snow was present on the ground.

Unfortunately, the closest weather station to Cimarron, which readily provided historical data, is approximately 50 miles (80 km) away in the city of Gunnison. Cimarron's elevation is also higher than that of Gunnison, and consequently the weather conditions (in particular the temperature) may be different at the slide site from that at the weather station, precipitation

occurred during the time of each ERS acquisition in 1997. However, given the importance of this data set to the study according to the slide movement that is known to have occurred, the satellite baseline data were judged to be sufficient to justify the data procurement even though precipitation was recorded on the day of each acquisition.

In the case of RADARSAT-1, acquisition planning began for this area in August 2003, with an Ascending Fine Mode F2F scene chosen for acquisition. In total, 26 acquisitions were captured over the site on this beam mode between August 2002 and June 2005. Within the scope of this project, scene selection was made on roughly a quarterly basis over the duration of the contract from September 2003 to June 2005. The scenes were collected with particular emphasis on minimizing the baseline (to less than 500 meters (1600 ft)) and choosing scenes on days without precipitation.

Ground movement maps were derived from the ERS and RADARSAT SAR interferogram. For individual interferograms, displacements that were less than 10 mm (0.4 inch) were considered to be within uncertainty levels. Movement greater than 10 mm (0.4 inch) were interpreted within the constraints associated with the phase variations and systematic uncertainties. Since areas of low temporal coherence stem from changes in the radar-scattering characteristics of the ground, such areas produced noisy interferometric phase. Further, systematic uncertainties may have arisen due to residual inaccuracies in the orbit modeling, atmospheric variations between the two acquisition times, and inaccuracies in the DEM and / or its co-registration to the SAR images. Except for small-scale atmospheric effects, these systematic variations were generally aligned with the topography and could therefore be identified. It was evident that all the ERS interferograms suffered from poor coherence, with mean values ranging from 8% to 20%. The displacement derived from these interferograms appeared to contain mostly small areas of noise that fluctuated by up to 20 to 30 mm (0.8 – 1.2 inch). Given the poor coherence and the absence of any consistent displacement signatures, one can only conclude that no movement was detected.

CHAPTER 7 – RECOMMENDATIONS

In the event that future monitoring using InSAR is attempted for this site, it is recommended that radar imagery be acquired from a satellite oriented with a much steeper viewing angle. The use of a steeper acquisition angle would likely increase the portion of the Amphitheatre Point AOI visible to the satellite, and decrease the degree to which geometric errors impede analysis.

A second recommendation is for the use of higher resolution radar data for any future monitoring projects, such as imagery captured from the TerraSAR-X or Cosmo SkyMed satellites. The use of higher resolution data may increase the ability of SqueeSAR™ to resolve additional features in the area, thereby increasing the number of potential radar targets.

Third, it is recommended that any future InSAR analyses planned for the Cimarron Landslide site use higher resolution radar data, captured from new satellites such as TerraSAR-X or Cosmo SkyMed. The acquisition of higher resolution imagery would allow for a more detailed analysis of the area and as a result, may allow for the extraction of additional radar targets within the Cimarron AOI.

Finally, for future projects that attempt to use InSAR in challenging areas, it is recommended that a Feasibility Study (FS) be carried out prior to a complete SqueeSAR™ analysis. In an FS a limited number of images are acquired (usually 8 for monitoring projects or 15 for the analysis of archive data) and processed to assess the density of radar targets that would be identified in an area if a full SqueeSAR™ analysis were to be carried out. This has the advantage of reducing the risk of an unsuccessful project by mitigating costs. Furthermore, if the FS is successful the images can usually be used in the subsequent SqueeSAR™ analyses, thereby recovering the costs of the imagery.

BIBLIOGRAPHY

- J. Allievi, C. Ambrosi, M. Ceriani, C. Colesanti, G.B. Crosta, A. Ferretti, D. Fossati “*Monitoring Slow Mass Movements with the Permanent Scatterers Technique*”, IGARSS 2003 – 21/25 July 2003 – Toulouse – France, pp. 1-3.
- C. Colesanti, A. Ferretti, F. Ferrucci, C. Prati, F. Rocca, “*Monitoring Known Seismic Faults Using the Permanent Scatterers (PS) Technique*”, Proceedings IEEE International Geoscience and Remote Sensing Symposium - IGARSS 2000, Honolulu (USA) 24-28 July 2000, Vol. 5, pp. 2221-2223.
- C. Colesanti, A. Ferretti, R. Locatelli, F. Novali, G. Savio, “*Permanent Scatterers: Precision Assessment and Multi-platform Analysis*”, IGARSS 2003 – 21/25 July 2003 – Toulouse – France, pp. 1-3.
- C. Colesanti, A. Ferretti, F. Novali, C. Prati, F. Rocca, “*SAR Monitoring of Progressive and Seasonal Ground Deformation Using the Permanent Scatterers Technique*” IEEE Transactions on Geoscience and Remote Sensing, Vol. 41, NO 7, July 2003, pp. 1685-1701.
- C. Colesanti, A. Ferretti, C. Prati, D. Perissin, F. Rocca, “*ERS-ENVISAT Permanent Scatterers Interferometry*”, IGARSS 2003 – 21/25 July 2003 – Toulouse – France, pp. 1-3.
- C. Colesanti, A. Ferretti, C. Prati, F. Rocca, “*Comparing GPS, Optical Levelling and Permanent Scatterers*”, Proceedings IEEE International Geoscience and Remote Sensing Symposium - IGARSS 2001, Sydney (Australia) 9-13 July 2001, Vol. 6, pp. 2622-2624.
- C. Colesanti, A. Ferretti, C. Prati, F. Rocca, “*Full Exploitation of the ERS Archive: Multi Data Set Permanent Scatterers Analysis*”, Proceedings IEEE International Geoscience and Remote Sensing Symposium - IGARSS 2002, Toronto (Canada) 24-28 June 2002.
- C. Colesanti, A. Ferretti, C. Prati, F. Rocca, “*Monitoring Landslides and Tectonic Motion with the Permanent Scatterers Technique*”, accepted by Engineering Geology, Special Issue on Remote Sensing and Monitoring of Landslides, in press.
- C. Colesanti, A. Ferretti, C. Prati, F. Rocca, “*Monitoring Landslides and Tectonic Motions with the Permanent Scatterers Technique*”, Engineering Geology, n. 68, 2003, pp. 3-14.
- C. Colesanti, A. Ferretti, C. Prati, F. Rocca, “*Seismic Faults Analysis in California by Means of the Permanent Scatterers Technique*”, Keynote Paper, Proceedings 3rd International Symposium on Retrieval of Bio- and Geophysical Parameters from SAR Data for Land Applications, Sheffield (United Kingdom) 11-14 September 2001, ESA SP-475, January 2002, pp. 125-131.
- C. Colesanti, R. Locatelli, F. Novali, “*Ground Deformation Monitoring Exploiting SAR Permanent Scatterers*”, Proceedings IEEE International Geoscience and Remote Sensing Symposium - IGARSS 2002, Toronto (Canada) 24-28 June 2002.

J.F. Dehls, M. Basilico, C. Colesanti, “*Ground deformation monitoring in the Ranafford area of Norway by means of the Permanent Scatterers technique*”, Proceedings IEEE International Geoscience and Remote Sensing Symposium - IGARSS 2002, Toronto (Canada) 24-28 June 2002.

T.H. Dixon, F. Amelung, A. Ferretti, F. Novali, F. Rocca, R. Dokkas, G. Sella, S.W. Kim, S. Wdowinski, D. Whitman, “*Subsidence and Flooding in New Orleans*”, Nature, Vol 441, 1st June 2006. pp. 587-588.

P. Farina, D. Colombo, A. Fumagalli, E. Gontier, S. Moretti, “*Integration of Permanent Scatterers Analysis and High Resolution Optical Images within Landslide Risk Analysis*”, FRINGE 2003 – 1/5 December 2003 – Frascati – Italy, pp. 1-8.

A. Ferretti, C. Colesanti, D. Perissin, C. Prati, F. Rocca, “*Evaluating the effect of the observation time on the distribution of SAR Permanent Scatterers*”, FRINGE 2003 – 1/5 December 2003 – Frascati – Italy, pp. 1-5.

A. Ferretti, C. Colesanti, C. Prati, F. Rocca, “*Radar Permanent Scatterers Identification in Urban Areas: Target Characterization and Sub-Pixel Analysis*”, Proceedings Joint IEEE/ISPRS Workshop on Remote Sensing and Data Fusion over Urban Areas, Roma (Italy) 8-9 November 2001, pp. 52.

A. Ferretti, C. Prati, F. Rocca, “*Analysis of Permanent Scatterers in SAR Interferometry*”, Proceedings of the IEEE International Geoscience and Remote Sensing Symposium, Honolulu (USA) 24-28 July 2000, Vol. 2, pp. 761 -763.

A. Ferretti, C. Prati, F. Rocca, “*Monitoring of Terrain Motion Using the PS Technique*”, Proceedings EUSAR2000 - 22 25 May 2000, Munchen, Germany, pp. 115-118.

A. Ferretti, C. Prati, F. Rocca, “*Monitoring Terrain Deformations Using Multi-Temporal SAR Images*”, Proceedings CEOS99 (Committee on Earth Observation Satellites) 26-29 October 1999 - Toulouse, France - <http://www.estec.esa.nl/CONFANNOUN/99b02/99b02.html>.

A. Ferretti, C. Prati, F. Rocca, “*Non-linear Subsidence Rate Estimation Using Permanent Scatterers in Differential SAR Interferometry*”, IEEE Trans. on Geoscience and Remote Sensing, Vol. 38, no. 5, September 2000.

A. Ferretti, C. Prati, F. Rocca, “*Non-Uniform Motion Monitoring Using the Permanent Scatterers Technique*”, Proceedings FRINGE99 - 10 12 November 1999, Liège, Belgium. <http://www.esa.int/fringe99/>.

A. Ferretti, C. Prati, F. Rocca, “*Permanent Scatterers in SAR Interferometry*”, IEEE Trans. on Geoscience and Remote Sensing, Vol. 39, no. 1, January 2001.

A. Ferretti, C. Prati, F. Rocca, “*Permanent Scatterers in SAR Interferometry*”, Proceedings EOS/SPIE Symposium on Remote Sensing - 20-24 September 1999 - Florence, Italy.

A. Ferretti, C. Prati, F. Rocca, “*Permanent Scatterers in SAR Interferometry*”, Proceedings “IGARSS’99” International Geoscience and Remote Sensing Symposium, 28 June-2 July 1999, Hamburg, Germany.

A. Ferretti, F. Ferrucci, C. Prati, F. Rocca, “*SAR analysis of building collapse by means of the permanent scatterers technique*”, Proceedings IEEE International Geoscience and Remote Sensing Symposium - IGARSS 2000, Honolulu (USA) 24-28 July 2000, Vol. 7, pp. 3219-3221.

A. Ferretti, C. Prati, F. Rocca, C. Colesanti, “*Validation of the Permanent Scatterers Technique in Urban Areas*”, Proceedings ERS - ENVISAT Symposium, Gothenburg (Sweden) 16-20 October 2000, - <http://www.esa.int/cgi-bin/envisat>.

B. Fruneau, C. Carnec, C. Colesanti, B. Deffontaines, A. Ferretti, S. Le Mouelic, A.M. Le Parmentier, J.P. Rudant, “*Conventional and PS differential SAR interferometry for monitoring vertical deformation due to water pumping: the Haussmann-St-Lazare case example (Paris, France)*”, FRINGE 2003 – 1/5 December 2003 – Frascati – Italy, pp. 1-6.

M. Guarnieri, “*ScanSAR interferometric monitoring using the PS technique*”, ERS ENVISAT symposium(Gothenburg, Sweden), 12-22 October, 2000.

M. Guarnieri, et al., “*Multi-Mode ENVISAT ASAR Interferometry: Techniques and Preliminary Results*”, in proc EUSAR 2002 (Cologne, Germany), May 4-6 2002, pp. 179-181, 2002.

M. Guarnieri, A. Ferretti, “*Visibility of Permanent Scatterers by ScanSAR*”, in proc EUSAR 2000 (Munich,Germany), May, 23-25, 2000, pp. 725-728, 2000.

M. Guarnieri, Y-L. Desnos, “*Optimizing performances of the ENVISAT ASAR ScanSAR modes*”, in proc IGARSS 99 (Hamburg, Germany), Jun. 28-Jul. 2, pp. 1758-1760, 1999.

G.E. Hilley, R. Bürgmann, A. Ferretti, F. Novali, F. Rocca, “*Dynamics of Slow-Moving Landslides from Permanent Scatterer Analysis*”, Science, Vol. 304, 25 June 2004.

A.O. Hohlhase, K.L. Feigl, D. Massonnet, A. Ferretti, “*Estimating orbital trajectories from fringe gradients in SAR interferograms for measuring crustal strain*”, IGARSS 2003 – 21/25 July 2003 – Toulouse – France, pp. 1-3.

P. Manunta, N. Casagli, D. Colombo, A.M. Deflorio, D. Spina, P.Farina, A. Ferretti, E. Gontier, K. Graf, S. Moretti, L. Olivier, M. Paganini, F. Palazzo, T. Strozzi, “*SLAM, a Service for Landslide Monitoring Based on EO-Data*”, FRINGE 2003 – 1/5 December 2003 – Frascati – Italy, pp. 1-6.

D. Power, J. Youden, J. English, K. Russell, S. Croshaw, R. Hanson “*InSAR Applications for Highway Transportation Projects*”, Publication No. FHWA-CFL/TD-06-002, April 2006, Federal Highway Administration, Central Federal Lands Highway Division, Lakewood, CO.

F. Prati, F. Rocca, A. Ferretti, C. Colesanti “*3D SAR Imaging for ground target recognition*”, Proceeding NATO Symposium on Complementarity of Ladar and Radar, Prague (Czech Republic) 22-23 April 2002.

F. Rocca, K.Daito, A. Ferretti, S. Kuzuoka, F. Novali, “*L-band PS analysis: JERS-1 results and TerraSAR - L predictions*”, FRINGE 2003 – 1/5 December 2003 – Frascati – Italy, pp. 1-6.

S. Sato, B. Kampes, M. Kooij, A. Place, “*InSAR Deformation Monitoring, General’s Highway, Sequoia National Park*”, Publication No. FHWA-CFL/TD-09-003, July 2009, Federal Highway Administration, Central Federal Lands Highway Division, Lakewood, CO.

B. Young, “*InSAR Deformation Monitoring, Badlands National Park*”unpublished, Federal Highway Administration, Central Federal Lands Highway Division, Lakewood, CO.

APPENDIX A – BASICS OF InSAR

INTERFEROMETRY

Interferometric Synthetic Aperture Radar (InSAR), also referred to as SAR Interferometry, is the measurement of signal phase change, or interference, over time. When a point on the ground moves, the distance between the sensor and the point on the ground also changes and so the phase value recorded by a SAR sensor flying along a fixed orbit will be affected, too. Figure 33 shows the relationship between that ground movement and the corresponding shift in signal phase between two SAR signals acquired over the same area.

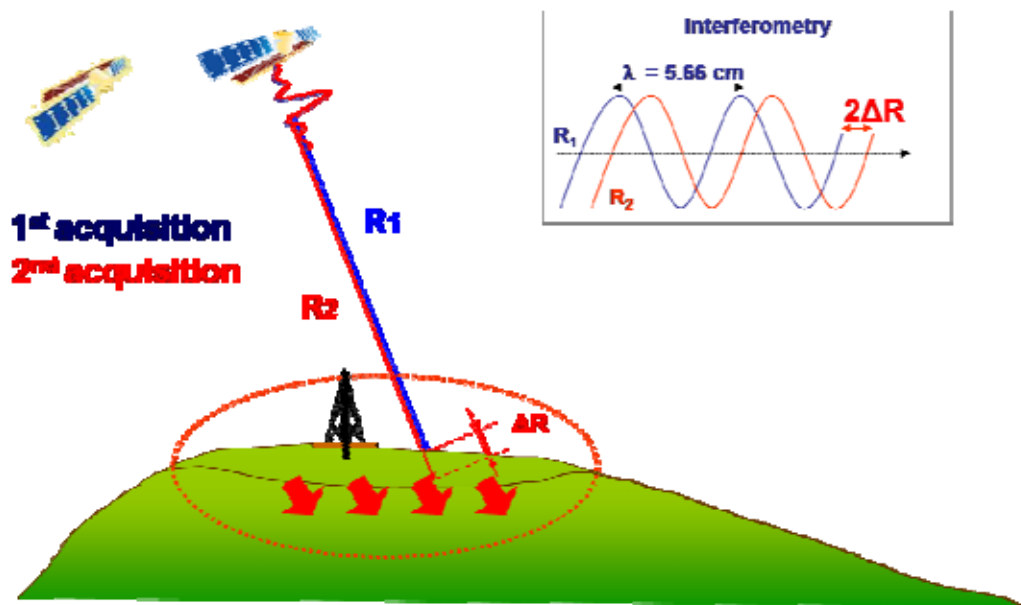


Figure 33. Schematic. A schematic showing the relationship between ground displacement and signal phase shift. The numerical value of the wavelength is that of ERS.

The change in signal phase ($\Delta\phi$) can be expressed in the form of the following simple equation:

$$\Delta\phi = \frac{4\pi}{\lambda} \Delta R + \alpha$$

Where λ is the wavelength, ΔR is the displacement and α is a phase shift due to different atmospheric conditions at the time of the two radar acquisitions. As a consequence, any displacement of a radar target along the satellite line of sight creates a phase shift in the radar signal that can be detected by comparing the phase values of two SAR images acquired at different times.

Apart from decorrelation effects, to be discussed in the next sections, SAR interferometry can only be applied in the following circumstances:

- Images have to be acquired by the same satellite using the same acquisition mode and properties (beam, polarization, off-nadir angle, etc);
- Images have to be acquired with the satellite in the same nominal orbit;
- The baseline separation between the master scene and any of the slave scenes must be no more than the “critical baseline” (a parameter that varies with the SAR sensor in use); the baseline being the distance between the satellite paths.

Interferograms

An interferogram is the difference of the phase values corresponding to a certain area, i.e. it is a digital representation of change in surface characterization. It is a matrix of numerical values ranging from $-\pi$ to $+\pi$ (since they correspond to phase variations) and it can be converted to a map – the easiest way to observe whether or not motion has occurred over a certain area.

Figure 34 is an interferogram of the L’Aquila earthquake that occurred in Italy, in April 2009. The colored bands, referred to as fringes, indicate areas where movement can be measured. The highly speckled areas indicate where some form of decorrelation arose. Here the noise level (mostly due to vegetation) prevents the application of InSAR and no useful information can be extracted. Data were acquired by the ENVISAT satellite for which one phase cycle corresponds to 28 mm of ground deformation along the line of sight (neglecting atmospheric effects).

The analysis of a SAR interferogram is not a trivial task to perform for non specialists. Apart from noise and decorrelation effects, interferometric phase values are a blend of different signal contributions, as will be discussed in the next section.

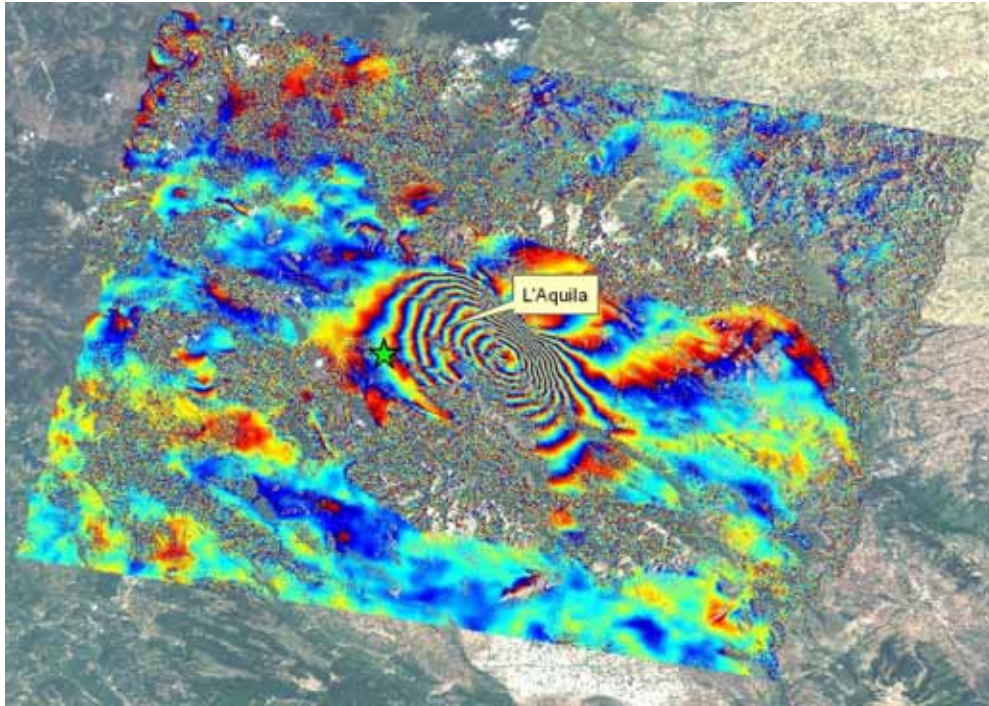


Figure 34. Map. An interferogram generated from two radar images one of which was acquired before the L'Aquila earthquake (February 2009) and the other shortly after the event (April 2009). The fringes indicate coherence whereby displacement can be calculated in the corresponding areas. The areas with a spotty appearance are areas where decorrelation noise has occurred. Phase values range from $-\pi$ to $+\pi$.

Contributors to Signal Phase

Interferometric phase ($\Delta\phi$) is impacted by four contributions: topographic distortions arising from slightly different viewing angles of the two satellite passes (t), atmospheric effects (α) arising from the wavelength distortion that occurs when signals enter and leave a moisture-bearing layer, any range displacement of the radar target (ΔR), and noise; range being the distance between the sensor and the target. More precisely:

$$\Delta\phi = \frac{4\pi}{\lambda} \Delta R + \alpha + t + noise$$

It is then clear that the difficulties related to the estimation of surface deformation signals from a single SAR interferogram are essentially due to the presence of decorrelation effects (contributing to the noise level), the impact of local topography on phase values and the presence of atmospheric phase components superimposed on the signal of interest. In Figure 34, most of the fringes visible in the interferogram are due to co-seismic deformation induced by the earthquake: in fact, the impact of the local topography has been removed, and atmospheric disturbances are not evident in this image.

Coherence

Interferometric fringes can only be observed where image coherence prevails. When an area on the ground appears to have the same surface characterization in all images under analysis, then the images are said to be coherent. If the land surface is disturbed between two acquisitions (e.g. an agricultural field has been ploughed, tree leaves have moved positions, etc.), those sub-areas will decorrelate in an InSAR analysis, resulting in noise and no information being obtainable. Coherence and correlation have the same meaning in this context. The term ‘noise’ is frequently used in this context and it is another word for non-coherence, or decorrelation. The fringes visible in Figure 34 reveal areas with high coherence while the speckled areas represent very low coherence and noise.

The coherence of an interferogram is affected by several factors, including:

- Topographic slope angle and orientation (steep slopes lead to low coherence)
- Terrain properties
- The time between image acquisitions (longer time intervals lead to lower coherence)
- The distance between the satellite tracks during the first and second acquisitions, also referred to as the baseline (larger baselines lead to lower coherence)

Typical sources of decorrelation are:

- Vegetation. Leaves grow and die and they also move. From one scene to the next, these changes are sufficient to change the appearance of the surface characterization. This is a particular problem for X-band and C-band sensors. L-band sensors can overcome this limitation in many situations, because their significantly longer wavelength is able to ‘see’ through foliage and reflect off objects beneath the vegetation and back through the foliage.
- Construction. At a construction site, the appearance of the land surface is changing constantly. This is a problem that is common to X-band, C-band, and L-band sensors.
- Erosion. Whether prompted by rain, snowmelt or wind, surface erosion will also change the surface characterization of land and, thereby, can decorrelate those areas where erosion is prevalent.
- Rapid Movement. Landslides and earthquakes precipitate rapid motion of an area of land. Quite often, the rapid motion causes destruction and, with it, a total change in the land surface’s appearance. With earthquakes, it is sometimes possible for rapid motion to occur without changes to surface characterization and, in those situations, interferometry can be successful. If the total movement occurring between successive image acquisitions exceeds one-half of the signal’s wavelength, decorrelation is likely to occur.

Coherence is measured by an index which ranges from 0 to 1. When an area is completely coherent, it will have a coherence value of 1. Correspondingly, if an area completely decorrelates, its coherence index will be 0. In general, interferometry is successful and accurate deformation is measurable when the coherence index lies between 0.5 and 1.0. Interferometry

can still produce meaningful results with coherence levels below 0.5 but as the index gets lower, so the results will display increasing levels of noise and may show erratic deformation patterns, from scene to scene, although movement trends are visible and generally reliable.

Wherever fringes occur, it is possible to calculate deformation by calculating the number of fringes and multiplying them by half of the wavelength. In the case of L'Aquila, C-band SAR was used and, therefore, each fringe should be multiplied by 28 mm (one-half of the wavelength) to calculate the total apparent displacement.

DIFFERENTIAL InSAR (DInSAR)

When a pair of images is subjected to interferometric analysis with a view to identifying movement and, thereafter, quantifying that movement, the process is referred to as Differential InSAR. Since change detection is now the goal, topographic effects are compensated for by using a Digital Elevation Model (DEM) of the area of interest, creating what is referred to as a differential interferogram (the word “differential” here refers to the subtraction of the topographic phase contribution from the SAR interferogram). The equation can then be represented as follows:

$$\Delta\varphi = \frac{4\pi}{\lambda} \Delta R + \alpha + \varepsilon + \text{noise}$$

Where ε is the contribution to phase arising from possible errors in the DEM that was used to remove the topographic effects.

Whenever the noise is low (i.e. decorrelation effects are negligible) and the phase contribution due to the local topography is accurately compensated for (i.e. ε is negligible as well), the interferometric phase can be simplified to the following equation:

$$\Delta\varphi = \frac{4\pi}{\lambda} \Delta R + \alpha$$

Where $\Delta\varphi$ is the *differential* interferometric phase, ΔR is the incremental distance the signal travels from the sensor to the ground and back, and α is the atmospheric contribution to phase shift.

Once the differential interferogram has been prepared, a deformation map can be created for all areas that are coherent.

In the mid-1990's, after extensive application of the DInSAR technology, the atmospheric contribution to phase shift was found to be significant, particularly in tropical and temperate areas. Unfortunately, there is no method for removing the α component, so users have to be aware of its effects. Thus, DInSAR should only be used on the understanding that deformation measurements are prone to errors arising from atmospheric circumstances. However, DInSAR, while not the tool for accurate displacement measurements, still has a use in identifying footprints of progressing movement. It can only measure total displacement between two points in time. Accordingly, it cannot distinguish between linear and non-linear motion.

INTERFEROGRAM STACKING

Following the realization that atmospheric effects on signal phase values were significant, a method emerged in the late 1990's that sought to mitigate this effect by 'averaging' data within multiple interferograms. This process was referred to as Interferogram Stacking.

By averaging the data in a stack of interferograms, the signal to noise ratio (SNR) values are enhanced and, theoretically, it is easier to extract information on displacement over longer periods of time than are realistic for single interferogram DInSAR.

However, for this process to work, certain assumptions are made:

- Although different versions of this technique exist, the displacement rate of the area of interest is assumed to be constant in time. In reality, such an assumption has limited validity. Multiple interferograms usually describe ground movement over time lines measured in years. Apart from tectonic deformation, linear movement over such time periods is not common.
- The data are heavily filtered, spatially, before the stacking procedure is implemented. Not only does this reduce the resolution but also prompts the loss of potentially valuable data contained in 'isolated' pixels with high SNR values, and it also smoothes out abrupt changes in displacement, e.g. seismic faults.
- The atmospheric contribution to signal phase is not estimated. Thereby, no assessment is possible on the quality of the filtering procedure. Atmospheric disturbances are characterized by specific statistical features, and the separation of motion and atmospheric phase components should take into account the peculiarities of the "noise" to be filtered out.
- Typically, stacking procedures are only applied using interferograms with an orbital baseline less than 300 m, because of the spatial filtering. As a result, substantial quantities of information that can be found from within interferograms whose baselines are as high as 1300 m are overlooked, the latter being a common baseline upper limit for PSI technologies.

While interferogram stacking provides the user with better information than can be obtained from single differential interferograms (DInSAR) the approach is far from optimal, particularly because deformation cannot be considered constant in time. Moreover, for the estimation of atmospheric noise, the procedure usually adopted to produce a weighted average, i.e. to assign different "importance" to different interferograms, is based on visual inspection of multiple interferograms.

Finally, as already mentioned, the estimation of errors is usually not performed.

PERSISTENT SCATTERER TECHNIQUES

General Concept

Persistent Scatterer Interferometry (PSI) is the collective term used within the InSAR community to distinguish between single interferogram DInSAR and the second generation of InSAR technologies, of which there are but a few. The first of these to appear, in 1999, was the PS Technique™, the base algorithm of which is PSInSAR™. The following description of PSI technology is based on the PSInSAR™ model.

All PSI technologies are advanced forms of DInSAR. In other words, the interferogram is at the core of PSI. The fundamental difference is that PSI technologies develop multiple interferograms from a stack of radar images. As a minimum, 15 radar scenes are usually required for PSI methods, including PSInSAR™, even though there are circumstances when an analysis can be conducted with fewer images (typically in urban areas). However, it should be noted that the more there are radar scenes available, the more accurate will be the results of PSInSAR™, and the same holds true for other PSI methods.

The main driver for the development of PSInSAR™ was the need to overcome the errors introduced into signal phase values by atmospheric artifacts. By examining multiple images, usually a minimum of 15 scenes, many interferograms (in this case 14 interferograms) are generated by selecting one of the scenes as a master to which the other 14 scenes become slaves.

The process by which removal of atmospheric effects is achieved involves searching the imagery and interferograms for pixels that display stable amplitude and coherent phase throughout every image of the data set. They are referred to as Permanent - or Persistent – Scatterers. Thus a sparse grid of point-like targets characterized by high signal to noise ratios (SNR) is identified across an area of interest on which the atmospheric correction procedure can be performed. Once these errors are removed, a history of motion can be created for each target.

Having removed the atmospheric artifacts, the interferometric data that remain are displacement values (resolved along the satellite LOS) plus noise, dependent on the quality (SNR) of the reflector.

Permanent Scatterers

A Permanent Scatterer (PS) is defined as a radar target, within a resolution cell, that displays stable amplitude properties and coherent signal phase, throughout all of the images within a data stack.

Sometimes a target may behave with a stable amplitude characteristic but its phase is erratic, or non-coherent. Further, some targets behave as if they are PS but only within a portion of the images within the data stack. Such targets are not PS.

Objects that make good PS are varied and can be natural or man-made. Among the natural forms are: rock outcrops, hard un-vegetated earth surfaces, and boulders. Among the man-made objects are: buildings, street lights, transmission towers, bridge parapets, above-ground pipelines, appurtenances on dams and roof structures, and any rectilinear structure that can create a

dihedral signal reflection back to the satellite. Figure 35 shows the results of a PSInSAR™ analysis of a man-made reservoir, in Italy. The colored dots represent the location of a PS, the color reflecting the displacement rate measured at that point.

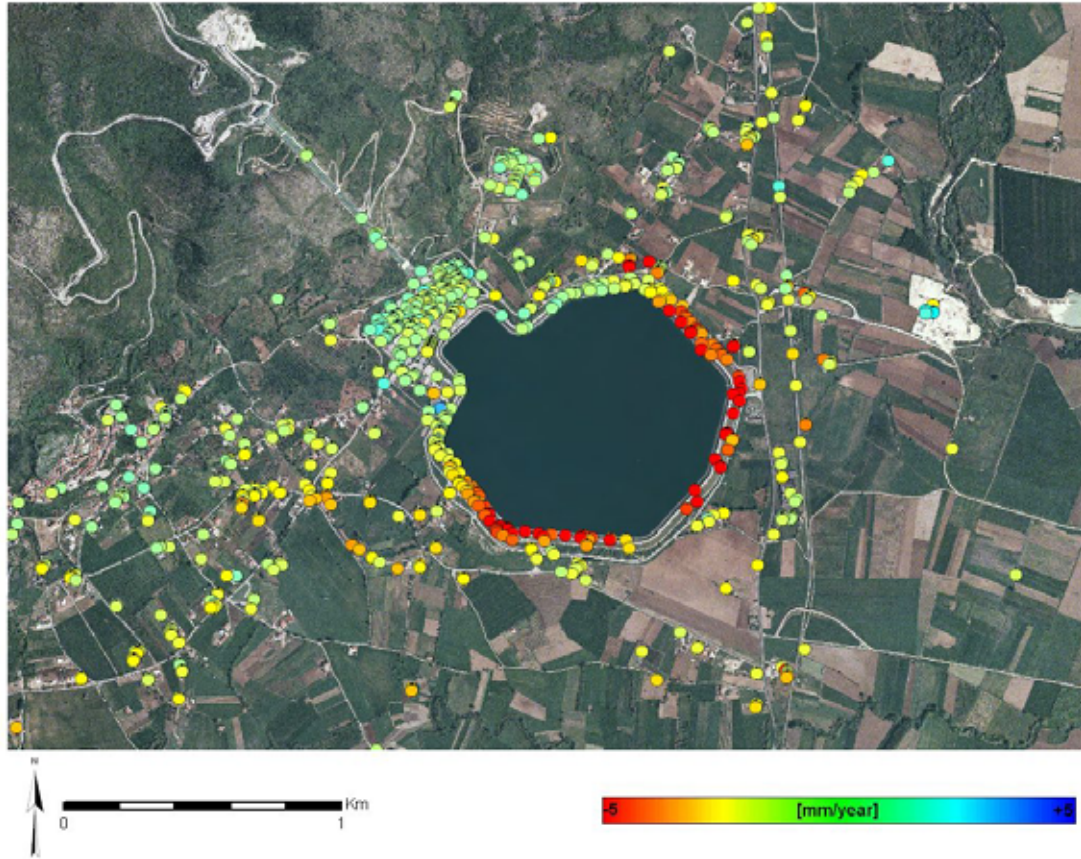


Figure 35. Map. The visual display of results of a PSInSAR™ analysis of Lake Presenzano and its surrounding area.

Calculating Displacement

All measurements are made in the LOS of the satellite’s radar beam and are relative to a point that is pre-selected as being stable and not moving (P_0). The selection of the reference point is best made conjunctively with an expert familiar with the area, the latter having better local knowledge on which sub-areas are stable within an AOI.

Once the data have been “cleaned up”, it is possible to develop the history of movement across the AOI. This is achieved by sequentially calculating the relative displacement between an individual radar target and the reference point, throughout the entire period of the analysis. Thus, the deformation is relative in time and space. A typical time series of movement of a PS is shown in Figure 36.

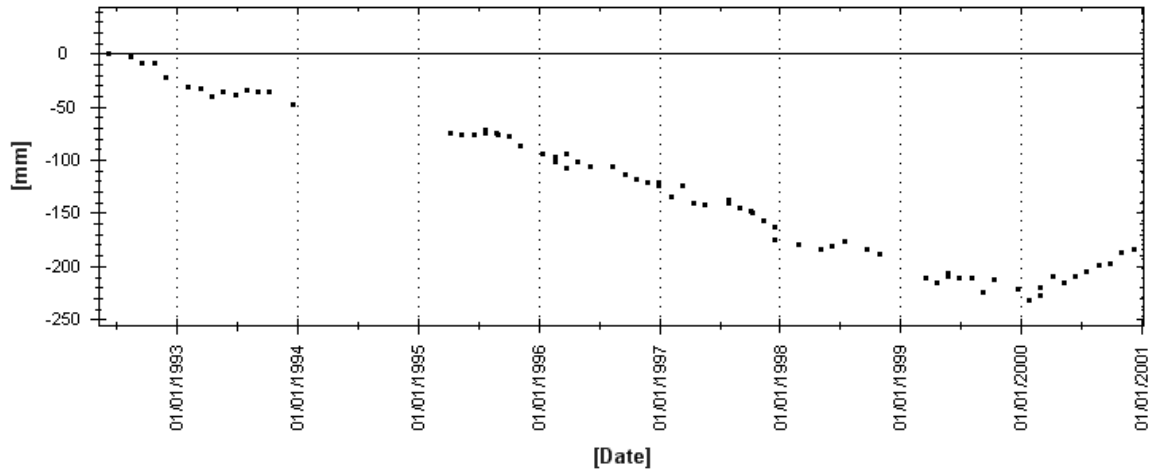


Figure 36. Graph. A typical time series showing linear and non-linear patterns of movement.

It should be noted that the PSInSAR™ algorithm generates a standard deviation map for the AOI, as well as providing error bar data for each PS, within the data base.

A priori information is always helpful before commencing a PS analysis. If an area is known to be subsiding, then measurement can be satisfactorily made using a single viewing geometry, also referred to as ‘acquisition mode’. However, if the hazard is a landslide, where significant horizontal movement might occur, the use of data acquired by satellites in both the ascending and descending orbits will enable true vertical movement and the East-West component of horizontal movement to be computed.

At the present time, it is not possible to determine the horizontal component of movement in the North-South direction. However, research is underway to try to solve this problem... Such computations will require the use of at least 3 data sets with differing viewing geometries and look angles.

Precision

Error bars of measurement of a PS are calculated as the deformation pattern is developed. However, precision of the displacement calculations is an important element in validating PS data. The most important factors impacting on data quality are:

- Spatial density of the PS (the lower the density, the higher the error bar)
- Quality of the radar targets (signal-to-noise ratio levels)
- Climatic conditions at the time of the acquisitions
- Distance between the measurement point (P) and the reference (P_0)

Figure 37 is a chart showing precision values obtained from many analyses of data from the ERS, Envisat, and RADARSAT-1 satellites.

<u>Displacement (LOS)</u>	Average Displacement Rate		Single Measurement
Precision (1s)	<1 mm/yr		5 mm
<u>Positioning</u>	E - W	N - S	Height
Precision (1s)	6 m	2 m	1,5 m

Figure 37. Table. Typical values of precision (1 sigma) for a point less than 1 km from the reference point (P₀), considering a multi-year dataset of radar images.

Comparable values for the satellites launched during 2007/8 are not yet available since the volume of data from these satellites that has been processed to date is still quite low. However, it is expected that precision will be improved because a) the sensors on the newer satellites are more sophisticated, and b) the resolution cell sizes are smaller than those of the earlier satellites.

Validation of PS Data

PS data have been compared with measurements obtained by other recognized measurement methods. However, it must be remembered that InSAR methods determine relative displacement, not absolute movement. Notwithstanding, it is possible to develop some comparisons and Figure 38, Figure 39 and Figure 40 show how PS data performed against Differential GPS and optical leveling surveys, as well as with thermal dilation modeling of buildings.

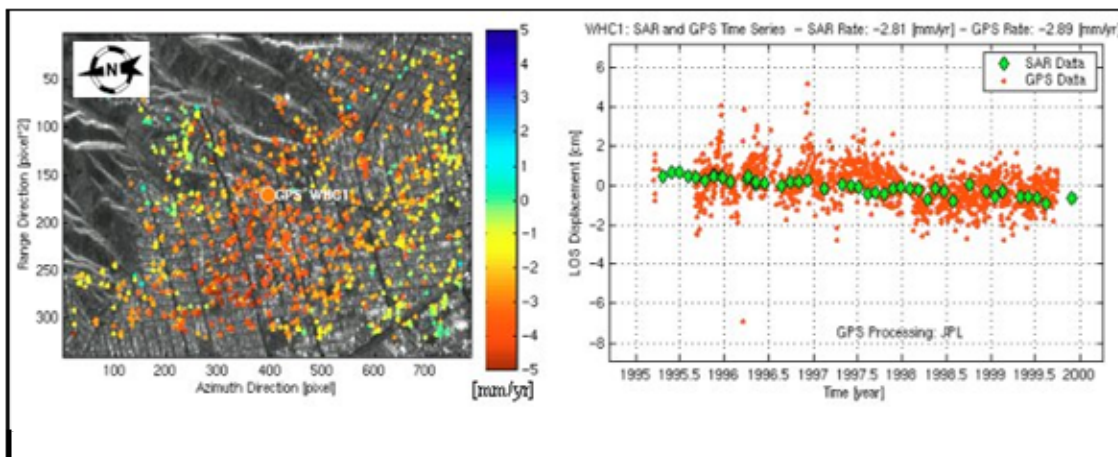


Figure 38. Graph. Comparison of PSInSAR™ with GPS data. The x, y and z components of GPS measurements have been resolved to the equivalent LOS of the satellite data.

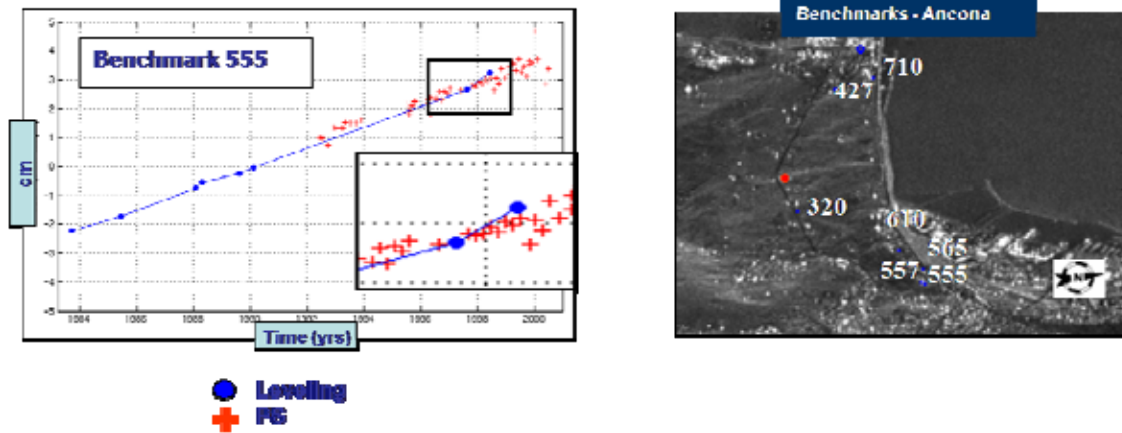


Figure 39. Graph. Optical leveling. The blue line is an optical benchmark correction curve; the red dots represent InSAR readings at the same location.

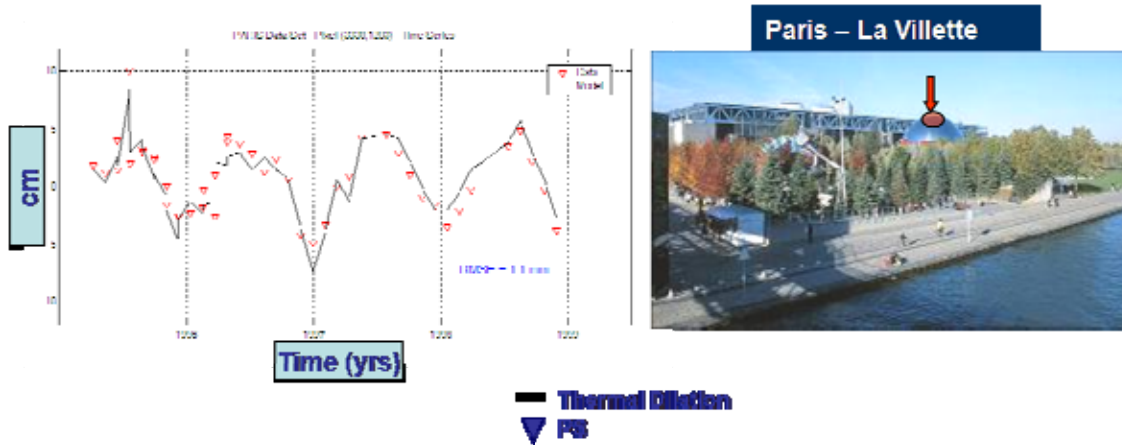


Figure 40. Graph. Thermal Dilation. Buildings move in response to changes in temperature and software is available to model such movement. The black line represents the results of a thermal dilation model while the red triangles correspond to InSAR readings on the same building, measured over the same time period.

Data Output and Presentation

The results of an InSAR analysis are best understood if they can be visualized and, in this regard, geographic information systems (GIS) are excellent tools.

The digital data are provided in ESRI shapefile format, which includes a database file, readable in most spreadsheet software, and can be used as input to downstream modeling exercises. Figure 41 shows a display of the database in which the location coordinates and displacement history of each PS is listed, along with other data about the particular PS, such as coherence, average velocity, acceleration, and height of the PS centroid relative to that of the reference point used in the PS analysis.

Visualization is possible using several forms:

- overlays on a digital orthophoto on a GIS
- overlays on an engineering drawing on a GIS
- overlays on a Google Earth platform
- on line hosting on a webGIS

All of these options allow the viewer to obtain close up and remote observation and, with the PSInSAR™ service, a software tool is provided to enable the viewer to point the cursor to any PS, click on it, and to view the pop up window showing the history of movement of that PS. Figure 41 (a-c) represents a sequence of screen grabs from a GIS showing the zooming features.

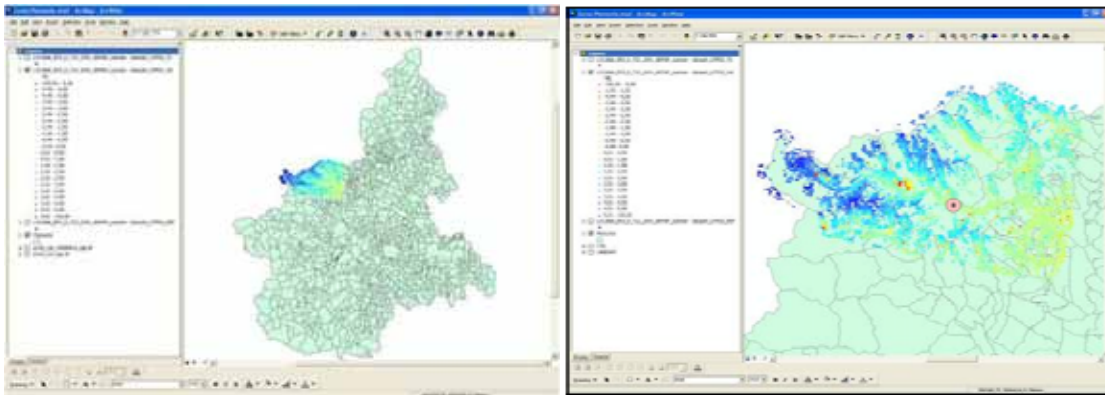


Figure 41 (a). Image. GIS area, showing PS. Figure 41 (b). Image. GIS close up of AOI.

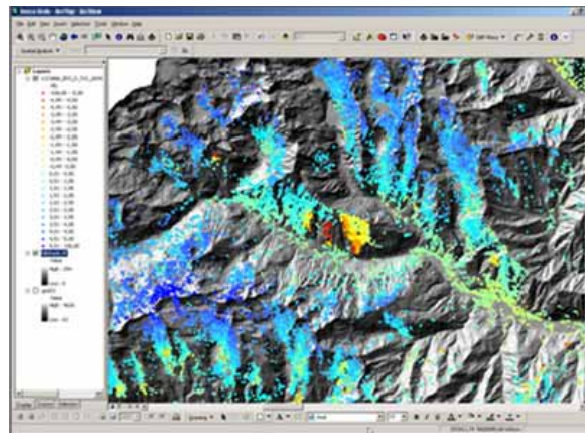


Figure 41 (c). Image. PS superimposed on topographical map.

Figure 41 (a-c). Image. These images are screen-grabs from a GIS showing how distant and close-up views of deformation phenomena can be observed using GIS platforms.

SqueeSAR™

In 2010, the new SqueeSAR™ algorithm was developed, which is an advance on the PSInSAR™ algorithm. SqueeSAR™ is a second generation PSInSAR™ analysis: exploiting both 'point wise' PS and 'spatially distributed scatterers' (DS). The new algorithm provides information in low-reflectivity homogeneous areas by identifying DS – previously unidentified with PSInSAR™.

DS are typically identified from homogeneous ground, scattered outcrops, debris flows, non-cultivated lands and desert areas. Figure 42 shows a schematic of the breakdown of the distribution of PS and DS over a typical AOI. PS (as identified with the previous algorithm PSInSAR™) usually correspond with man-made objects. DS, as described above, are only identified with the latest SqueeSAR™ algorithm and correspond to homogeneous areas of ground. Satellite signals are not returned over heavily vegetated areas.

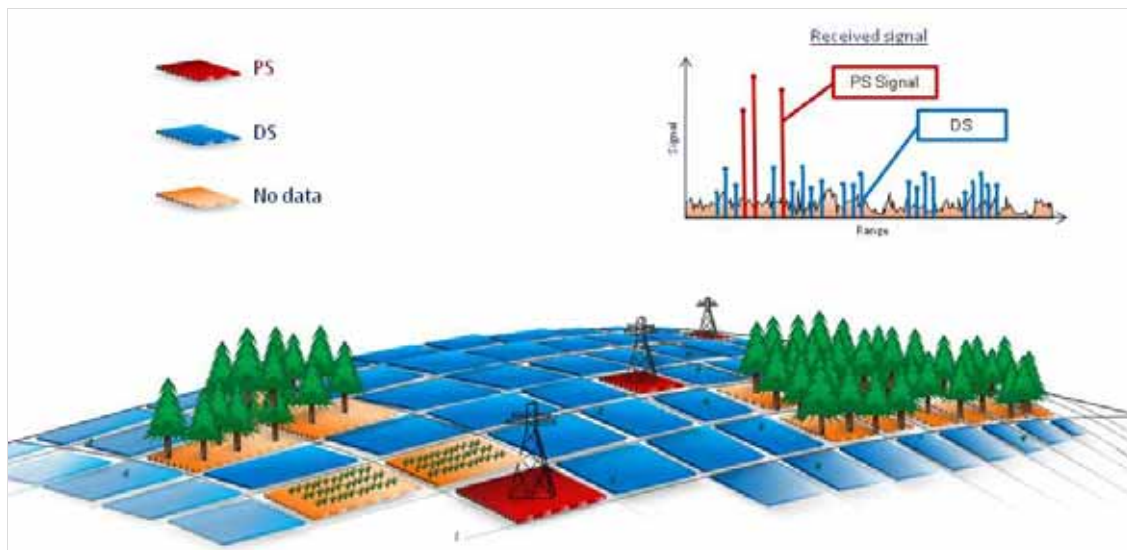


Figure 42. Schematic. Schematic showing the distribution of PS and DS over a typical AOI. PS are identified as single objects returning a strong signal to the satellite. DS are homogeneous areas or scattered outcrops. Areas heavily covered by vegetation do not return the satellite signal.

SqueeSAR™ is inclusive of the PSInSAR™ algorithm, providing a significantly increased coverage of ground points, especially over non-urban areas. Figure 43 shows a comparison between the number of ground points identified using the previous PSInSAR™ algorithm and the latest SqueeSAR™ algorithm.

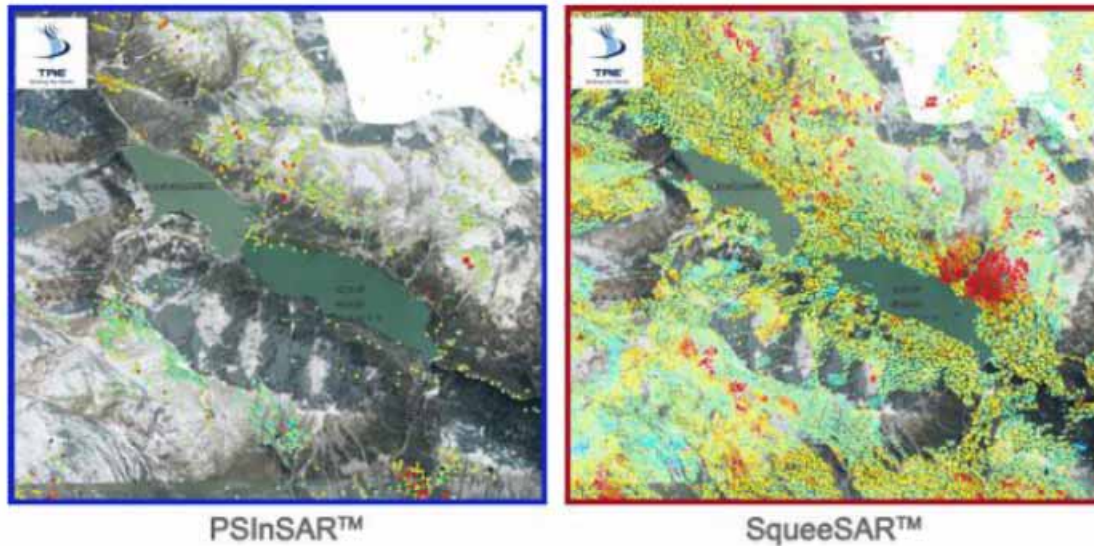


Figure 43. Map. Comparison between the number of ground points identified using PSInSAR™ (previous algorithm identifying only PS) and SqueeSAR™ (latest algorithm identifying both PS and DS). There is a significant increase in the number of identified ground points.

SqueeSAR™ exploits both PS and DS, providing a significantly higher density of ground points and hence coverage of ground displacement over the AOI. A summary of the benefits of SqueeSAR™ are given below:

- both PS and DS ground measurement points identified
- high density of ground points supplied
- time-series provided for each ground point identified
- millimetre accuracy on ground displacement values
- time-series standard deviation reduced compared to previous algorithm i.e. coherence increased and noise decreased
- increased confidence on ground behaviour due to increased coverage of points – especially significant for generic areas with low reflectivity

Since its introduction in 2010, as the replacement to the widely accepted PSInSAR™ algorithm, SqueeSAR™ has challenged the industry standard by identifying many more ground points, and hence increasing overall understanding of ground displacement occurring in an AOI.

APPENDIX B – RADAR COHERENCE

Figure 44 displays the coherence values over the Amphitheatre Point Landslide area, and Figure 45 displays the coherence values over the Cimarron Landslide area.

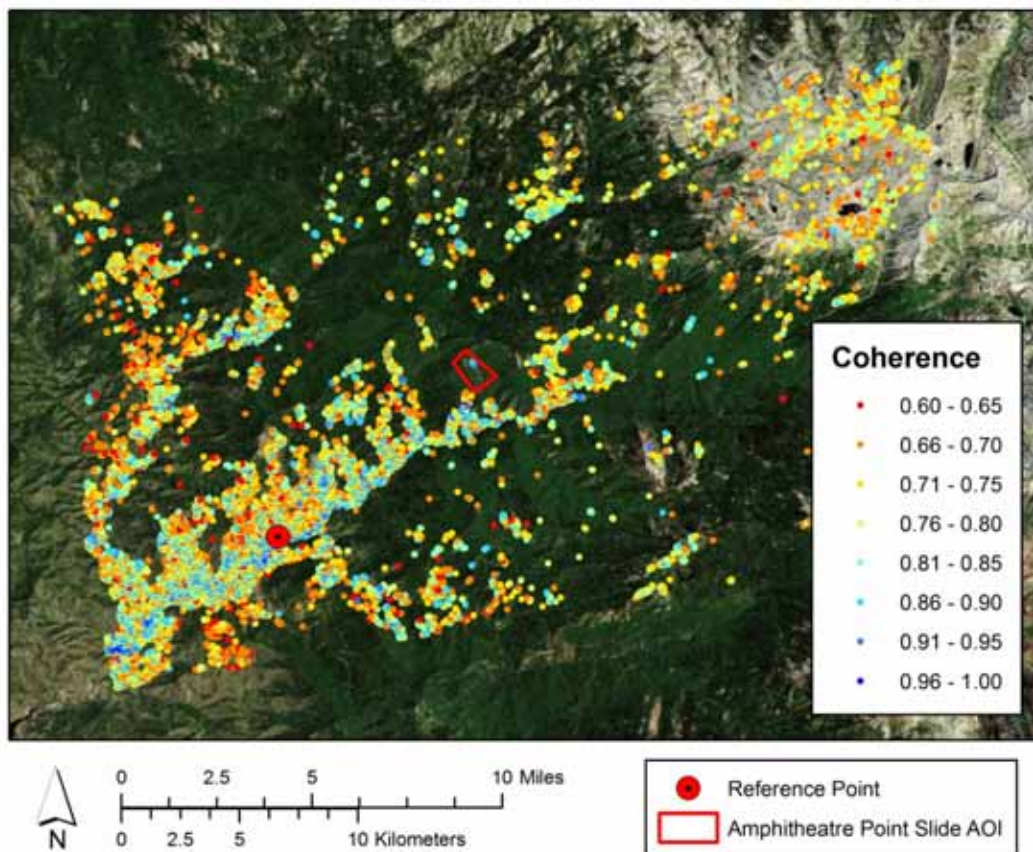


Figure 44. Map. Coherence of the radar targets before data filtering within the processed Amphitheatre Point Landslide area.

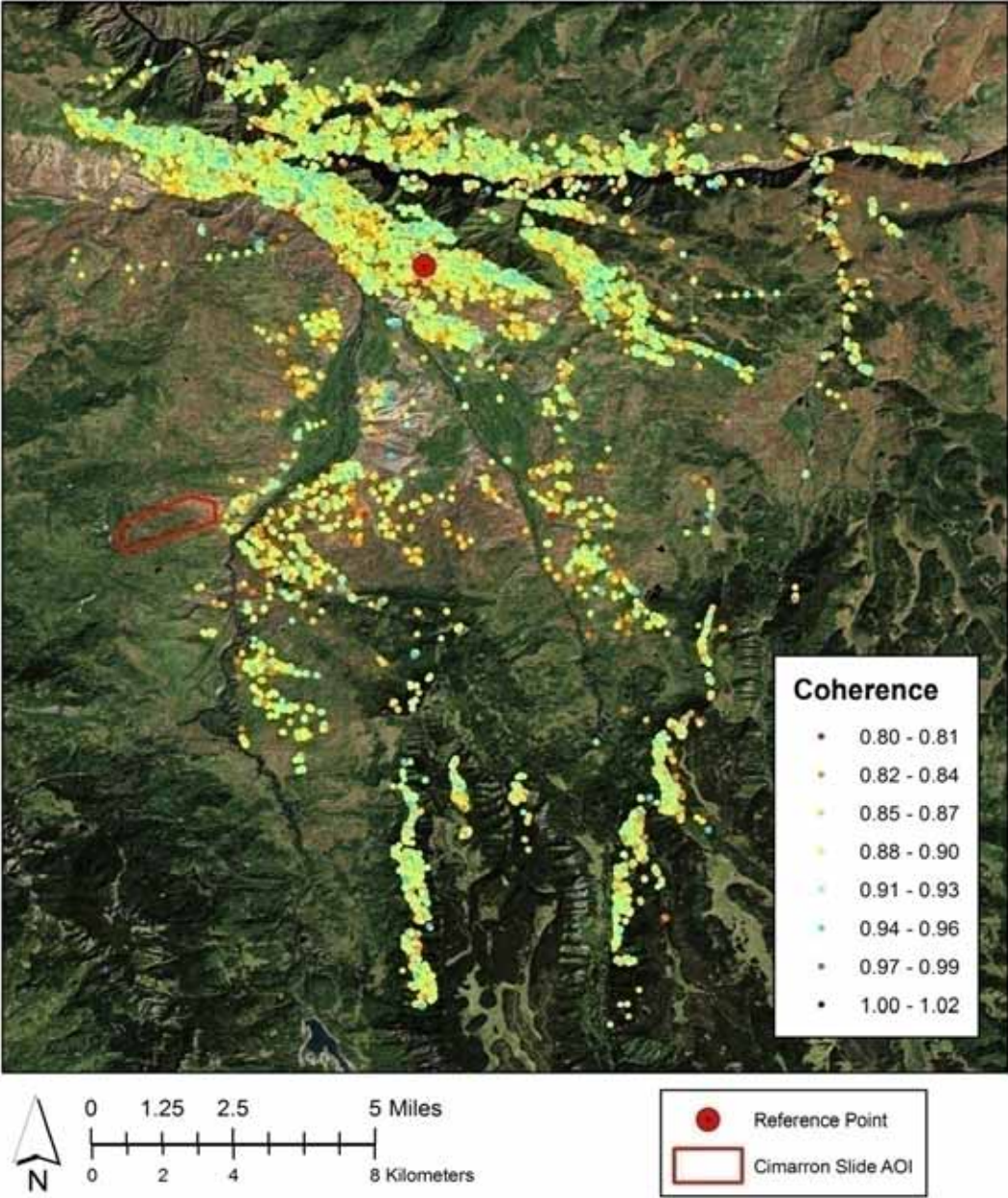


Figure 45. Map. Coherence of the radar targets within the processed Cimarron Landslide area.

APPENDIX C – AMPLITUDE MAPS

The MIR image derived from the Amphitheatre Point Landslide image archive is shown in Figure 46. The MIR image derived from the Cimarron Landslide image archive is shown in Figure 47.

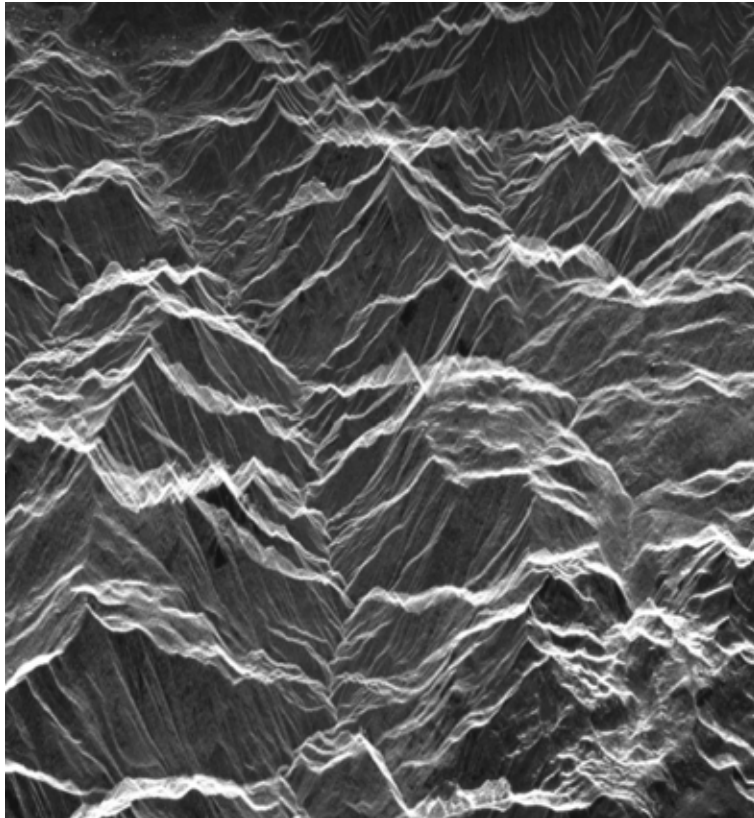


Figure 46. Map. Multi-image reflectivity map of the Amphitheatre Point Landslide area. North is pointing to the right side of the image.



Figure 47. Map. Multi-image reflectivity map of the Cimarron Landslide area. North is pointing to the left side of the image.

